Icarus 417 (2024) 116120

Contents lists available at ScienceDirect

Icarus

journal homepage: www.elsevier.com/locate/icarus

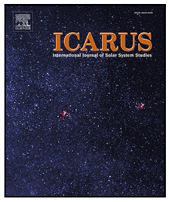

Research Paper

Exploring the tidal responses of ocean worlds with PyALMA^3

Flavio Petricca [a,b,*], Saikiran Tharimena [b,c], Daniele Melini [d], Giorgio Spada [e], Amirhossein Bagheri [f], Marshall J. Styczinski [g], Steven D. Vance [b]

[a] Department of Mechanical and Aerospace Engineering, Sapienza University of Rome, Italy
[b] Jet Propulsion Laboratory, California Institute of Technology, USA
[c] Schibsted ASA, Norway
[d] Istituto Nazionale di Geofisica e Vulcanologia, Italy
[e] Dipartimento di Fisica e Astronomia "Augusto Righi", Università di Bologna, Italy
[f] Division of Geological and Planetary Sciences, California Institute of Technology, USA
[g] Blue Marble Space Institute of Science, USA

ARTICLE INFO

Keywords:
Galilean satellites (627)
Tides (1702)
Planetary interior (1248)
Ocean planets (1151)

ABSTRACT

Observations of the tidal response of celestial bodies quantified by the Love numbers are highly relevant in planetary geophysical investigations because they provide unique insight into the interior structures. For example, the high sensitivity of tidal deformations to the properties of the oceans detected beneath the icy surfaces of some moons is of paramount importance for investigations of their habitability. We present here PyALMA^3, a software framework developed in Python devoted to the computation of planetary Love numbers. PyALMA^3 is based on ALMA^3, a previous version developed in Fortran. Conversion to Python significantly improves the accessibility and portability of the software. We tested PyALMA^3 by applying it to the exploration of the tidal responses of Europa and the other Galilean moons. We show that accurate modeling of effects such as the viscoelastic deformations of ice and the water density gradient in the ocean (variations of 2–3% on the real part of k_2) will be important in the context of geophysical investigations that will be conducted by future missions targeting icy moons, such as Europa Clipper and JUICE.

1. Introduction

Celestial bodies are periodically perturbed by external or surface forcings that deform their shape and change their gravitational potential. To describe these planetary deformations and relate them to the forcing, the Love number formalism was introduced (Love, 1911). Three different sets of Love numbers describe the response to the main perturbation mechanisms in terms of radial and horizontal surface deformations, and variations in the total gravitational potential. The tidal Love numbers quantify the perturbations induced by gravitational tides raised by an external potential, while the load Love numbers and the shear Love numbers describe the response to a normal and tangential surface load, respectively (*e.g.,* Farrell, 1972). Since the deformations and the induced response strongly depend on the interior structure of the body, measurements of the Love numbers can provide significant constraints on the internal structure of planetary bodies. For example, with the dearth of seismic measurements for most of the celestial bodies, detection of the tidal response through observation of the tidal Love numbers can provide clues on the state of planetary cores (*e.g.,* Yoder et al., 2003; Dumoulin et al., 2017), or evidence for existence of subsurface oceans in icy moons (*e.g.,* Moore and Schubert, 2000; Iess et al., 2012). In particular, due to the considerable influence of the oceans on tidal deformations, the Love numbers represent a powerful way to sound the structure and thermal state of ocean worlds, revealing valuable clues about their habitability (Vance et al., 2018).

To infer constraints on the interior properties of a body, it is necessary to model the planetary deformations induced by a generic forcing and compare the results to the observations. Love numbers can be computed in the framework of the gravito-elastic theory, which describes the deformations of a spherically symmetric self-gravitating body in response to gravitational tides, surface loading and traction, or free oscillations of the body. The mathematical formalism was first developed to study the elastic response of the Earth to oscillations generated by an earthquake (Alterman et al., 1959; Takeuchi and Saito, 1972), and consists of a set of six first-order differential equations resulting from the equilibrium equations of a solid body (conservation of mass and momentum) coupled with the Poisson equation for the gravitational potential. This formulation can be straightforwardly extended to a viscoelastic body by invoking the Correspondence Principle (Biot,

* Corresponding author at: Jet Propulsion Laboratory, California Institute of Technology, USA.
E-mail address: flavio.petricca@jpl.nasa.gov (F. Petricca).

https://doi.org/10.1016/j.icarus.2024.116120
Received 24 January 2024; Received in revised form 1 May 2024; Accepted 2 May 2024
Available online 9 May 2024

1954). The Love numbers can then be computed by solving the Laplace-transformed set of equilibrium equations by using the normal modes approach (Peltier, 1974). Melini et al. (2022) presented ALMA^3, a software written in Fortran that enables the evaluation of the viscoelastic Love numbers of a layered spherically symmetric planet by adopting the normal modes technique. ALMA^3 extends the functionalities of the previous version (Spada, 2008) by adding several new functions, including the capability to compute frequency-dependent Love numbers, which describe the response to periodic forcing, new rheology models, and the possibility to model a layered core. These features make ALMA^3 very useful for planetary geophysical investigations, for which observation and interpretation of the response to periodic forcing such as gravitational tides or surface loading represent important objectives toward a better understanding of planetary interiors and evolution. ALMA^3 has already been used to compute the Love numbers of multiple planetary bodies, including the Moon (Briaud et al., 2023a,b), Mercury (Goossens et al., 2022), Venus (Saliby et al., 2023; Petricca et al., 2022), Mars (Petricca et al., 2022), and Enceladus (Genova et al., 2024).

Here, we present PyALMA^3 (Styczinski et al., 2024), a planetary-oriented Python software framework based on ALMA^3 to compute the frequency-dependent Love numbers of a spherically symmetric celestial body. The conversion to Python significantly improves the accessibility and portability of the code, enabling an easier integration with other Python frameworks devoted to planetary interior modeling, such as *PlanetProfile* (Styczinski et al., 2023a). We introduce PyALMA^3 in combination with a methodology based on a Monte Carlo scheme useful to study the dependency of the tidal Love numbers on the interior properties by exploring a large parameter space. We show that this approach, enabled by the efficient numerical scheme adopted by PyALMA^3, can be very valuable in understanding the relationship between geophysical parameters and the interior structure of a body, and thus the information that can be obtained through measurements of these quantities. We applied this methodology in combination with PyALMA^3 to investigate the tidal response of Jupiter's moon Europa. We focus on the influence of effects relevant to the tidal modeling of ocean worlds, such as viscoelastic response of ice and the effect of density variations with depth in the ocean, and we show that they need to be properly modeled to interpret the measurements that will be acquired by future missions.

This paper is structured as follows: Section 2 introduces to the methods used by PyALMA^3 to compute the Love numbers for a viscoelastic planet, the rheological models included in the software and the interior modeling that we use to benchmark PyALMA^3 and study the tidal response of Europa. Section 3.1 presents a validation benchmark of the software by comparing the Love numbers computed for a viscoelastic model of Europa with PyALMA^3. Section 3.2 shows the results of the investigation of Europa's tidal response carried out with PyALMA^3. An application of PyALMA^3 to Europa, Ganymede, and Callisto to investigate the effects of water density gradient on their tidal response is presented in Section 3.3. Finally, we discuss and summarize the relevance of PyALMA^3 and the effects on tidal modeling that we quantified in the context of future missions in Sections 4 and 5.

2. Methods

This section introduces the rheological models commonly used in planetary applications to describe the response to loading or tidal forcings, and the methods that we use to build interior models to benchmark PyALMA^{3}and explore the tidal responses of ocean worlds. The subsection on rheological models focuses on the improvements of PyALMA^{3}with respect to ALMA^3, including a generalization of the Andrade rheology and the implementation of the Sundberg-Cooper rheology.

2.1. Rheological models

The response of a particular viscoelastic material to an external forcing can be described in the Laplace domain with the same formalism as the elastic problem, in which the elastic shear modulus μ is replaced by a function $\mu(s)$, related to the constitutive equation of the material. In the context of the propagator approach to compute planetary Love numbers, the complex shear modulus is contained in the propagators $\Lambda(s)$ (see Appendix A). In general, deformations in a solid body subject to shear loading follow a sequence driven by three regimes (*e.g.,* Jackson et al., 2014; Renaud and Henning, 2018; Bagheri et al., 2022a): after instantaneous and recoverable elastic and anelastic deformations that are relevant on short time scales (regime 1), a transient creep regime is achieved (regime 2), ultimately followed by steady-state creep (regime 3), in which the response is fully viscous. Rheological models describe this response in the time domain using a creep function, which accounts for the different regimes of the viscoelastic response. The complex creep compliance $J(s)$ is the Laplace transform of the time-domain creep function $J(t)$ and its reciprocal is the complex shear modulus $\mu(s) = 1/J(s)$.

Simple viscoelastic models can reproduce only the instantaneous elastic and steady-state viscous regimes. For example, the Maxwell model has been widely used for Earth (*e.g.,* Peltier, 1974) and planetary applications (*e.g.,* Moore and Schubert, 2000; Bills, 2005). However, this rheology does not appropriately reproduce the observed dependence of material dissipation on the forcing period. Several rheological models have been proposed through laboratory experiments and physical principles to more accurately characterize the response of planetary materials (*e.g.,* ice and rocks), including the Andrade model (Andrade, 1910; Castillo-Rogez et al., 2011) and the Sundberg–Cooper model (Sundberg and Cooper, 2010; Renaud and Henning, 2018). The fundamental advantage of these models over simpler rheologies such as Maxwell is that they are able to reproduce the response associated with transient creep, occurring at timescales intermediate between the elastic and viscous regimes. This range of forcing periods is relevant to many tidal interactions within the Solar System, leading to a better description of the response to gravitational tides. Specifically, application of these rheological laws to modeling of Mars's tidal response showed that they can fit geophysical observations with a plausible mantle viscosity structure, whereas the Maxwell model yields viscosities too low to match observations (Bagheri et al., 2019; Bills, 2005; Nimmo and Faul, 2013). Compared to the Maxwell model, the transient components of these rheology models can produce a greater tidal heating by an order of magnitude, with important implications for the thermal and orbital evolution of Galilean moons and exoplanetary systems (Renaud and Henning, 2018; Renaud et al., 2021). As a result, these models have been widely used in modeling planetary response in recent years, both for rocky (*e.g.,* Dumoulin et al., 2017; Padovan et al., 2014; Goossens et al., 2022) and icy bodies (*e.g.,* Castillo-Rogez et al., 2011; Rambaux et al., 2010; Gevorgyan et al., 2020; Bagheri et al., 2022b).

The Andrade and Sundberg–Cooper rheologies reproduce the response associated with transition between the elastic and the fully viscous regimes through the inclusion of transient components in the complex creep compliance and shear modulus. The complex shear modulus for a Maxwell model consists of only the elastic and viscous terms:

$$\mu(s) = \frac{\mu s}{s + \mu/\eta} \tag{1}$$

where μ is the unrelaxed shear modulus (*i.e.,* the material response shortly after the application of the stress) and η is the Newtonian viscosity, which describes the response when the fully viscous regime is achieved. In the Maxwell model, the transition between the elastic and viscous response occurs at a characteristic relaxation time called the Maxwell time $\tau_M = \eta/\mu$. In contrast, the Andrade and Sundberg–Cooper models include transient terms and feature a distribution of relaxation

times instead of a single value. The Andrade complex shear modulus is given by (*e.g.* Melini et al., 2022; Goossens et al., 2022):

$$\mu(s) = \frac{\mu s}{s + \mu/\eta + s\mu^{\alpha}\Gamma(\alpha+1)(s\eta\zeta)^{-\alpha}} \tag{2}$$

where Γ is the Euler's gamma function and α is an empirical parameter that describes the duration of the transient response. Its value has been observed to be in the range $0.2-0.4$ from laboratory evidence and it has been found that this range provides a good fit to the experimental data for both rocks and ice (*e.g.,* Castillo-Rogez et al., 2011). The parameter $\zeta = \tau_A/\tau_M$ is the ratio between the Andrade characteristic time τ_A (on which anelastic creep occurs) and the Maxwell time (Efroimsky, 2012; Renaud and Henning, 2018). An alternative formulation of the Andrade model is based on the parameter β, which describes the strength of anelastic dissipation and can be related to the other parameters of the rheological law by:

$$\beta = \zeta^{-\alpha}\mu^{-1}\tau_M^{-\alpha} \tag{3}$$

Under low stress regimes, β was fit to experimental data in the pioneering work by Castillo-Rogez et al. (2011), who introduced the Andrade model in planetary applications and showed that the β parameter is approximated by:

$$\beta \approx \mu^{\alpha-1}\eta^{-\alpha} \tag{4}$$

Comparing Eqs. (3) and (4), it is clear that this approximation is equivalent to assuming $\zeta = 1$. In this case, the anelastic and viscous timescales are equal. However, Castillo-Rogez et al. (2011) emphasize that the fit to the experimental data that yields $\zeta \simeq 1$ is only valid in a specific range of $\mu^{\alpha-1}\eta^{-\alpha}$, and therefore it should be used with caution. Recent efforts proposed a broader range for ζ, varying between $1\times10^{-2}-1\times10^{1}$ (Bierson, 2024; Walterová et al., 2023), although values as high as 1×10^{5} are still consistent with geodetic measurements of the Earth's Love and Shida numbers (Amorim and Gudkova, 2024).

ALMA^3 extended the functionalities of previous versions by including the Andrade rheology with $\zeta = 1$. Given the uncertainties in the parameter ζ, in PyALMA^3 we have included the possibility of choosing different values for ζ for each layer described by an Andrade rheology. We have also augmented the set of rheologies available in PyALMA^3 by including the Sundberg–Cooper model. The expression of the complex shear modulus described by this rheological model is (Renaud and Henning, 2018; Goossens et al., 2022):

$$\mu(s) = \frac{\mu s(\overline{\mu}/\overline{\eta} + s)}{s^2(1+\mu^{\alpha}\Gamma(\alpha+1)(s\eta\zeta)^{-\alpha}) + s(\mu/\eta + (\mu+\overline{\mu})/\overline{\eta} + \overline{\mu}/\overline{\eta}\,\mu^{\alpha}\Gamma(\alpha+1)(s\eta\zeta)^{-\alpha}) + \mu\overline{\mu}/(\eta\overline{\eta})} \tag{5}$$

where $\overline{\mu}$ is the defect shear modulus (Renaud and Henning, 2018) and $\overline{\eta}$ is the Voigt–Kelvin viscosity. PyALMA^3 allows the user to choose the parameters α, ζ, $\overline{\mu}$ and $\overline{\eta}$ for every layer of the interior model.

2.2. Interior structure modeling

Our interior models are based on a four-layer structure for Europa, including a rock–iron core, an ocean, and an outer ice I shell. The ice shell is divided into a lower/warm and an outer/cold portion. The warm shell is representative of the ice layer that is subject to ductile deformations, in which subsolidus convection occurs, while the cold layer undergoes brittle deformations and transfers heat entirely by conduction.

2.2.1. Monte Carlo sampling

Some properties of Europa's interior layers have been constrained by previous work with measurements of the moon's gravity and magnetic fields acquired by Galileo (*e.g.,* Anderson et al., 1998; Hand and Chyba, 2007; Gomez Casajus et al., 2021; Petricca et al., 2023; Zimmer et al., 2000). However, given the sparsity of these data, large uncertainties affect our knowledge of the interior structure, especially the thickness of the ice shell, which has been suggested to range between a few km and 100 km (*e.g.,* Ojakangas and Stevenson, 1989; Hussmann et al., 2002; Howell, 2021; Vilella et al., 2020; Bray et al., 2014). Our objective here is to explore the tidal response of Europa and investigate the sensitivity of the tidal Love numbers to different properties of the interior. To do this, we vary the interior properties in a broad range without any *a priori* assumption on them. We build our models by randomly varying the interior properties with a Monte Carlo sampling algorithm. Our 11-dimensional parameter space includes the size, density, and rheological properties of the layers (Table 2). For each parameter, we build uniform prior probability distributions across the range presented in Table 2. From each distribution we draw a random sample and use these samples to build an interior model. With this approach, we generate a large number of models ($\mathcal{O}(10^7)$), which allows us to map the parameter space by exploring a large number of combinations between the interior properties. The core density $\rho_{\rm core}$ is adjusted to match the total mass ($M = 4.8\times10^{22}$ kg, Table 1), while the ice density $\rho_{\rm ice}$ is assumed to be equal to 917 kg m^{-3} (Fukusako, 1990). Once all the models are built, we filter them by excluding all models not in agreement with the MoI derived by Gomez Casajus et al. (2021) from Galileo radio science data to within 3 standard deviations (Table 1). Discarding models with this approach implies assuming that the MoI is uniformly distributed in the credible interval within 3 standard deviations from the central value (*i.e.,* $0.3547 \pm 3\times0.0024$ for the axial MoI, C/MR^2). Prescribing the consistence of the MoI with observational evidence with this approach results in an acceptance rate of 5% (~500 000 accepted models).

Table 1
Observations that we used to constrain our interior modeling of the Galilean satellites. The moment of inertia is considered with the measurement uncertainty, while the mass and radius of the interior models are enforced to be equal to the observed value.

	Radius [km]	Mass ($\times10^{22}$ kg)	Moment of Inertia (C/MR^2)
Europa	1560.8	4.8	0.3547 ± 0.0024
Ganymede	2631.2	14.8	0.3115 ± 0.0028
Callisto	2410.3	10.8	0.3549 ± 0.0042

Table 2
Summary of properties considered for our interior models of Europa. All properties are assumed to be random variables, with priors given by uniform distributions throughout the range presented here.

Parameter	Range	Units	Symbol
Ocean depth	0 – 200[a]	km	$d_{\rm ocean}$
Conductive ice shell thickness	0 – 150[b]	km	$d_{\rm ice,cond}$
Convective ice shell thickness	0 – 150[b]	km	$d_{\rm ice,conv}$
Ocean density	1000 – 1300[c]	kg m^{-3}	$\rho_{\rm ocean}$
Core shear modulus	50 – 70[c]	GPa	$\mu_{\rm core}$
Ice shear modulus	2.5 – 4.5[d]	GPa	$\mu_{\rm ice}$
Core viscosity exponent	18 – 22[ef]	$\log_{10}$(Pa s)	$\eta_{\rm core}$
Melting point ice viscosity exponent	12 – 16[g]	$\log_{10}$(Pa s)	$\eta_{\rm ice,melt}$
Creep activation energy	50 – 70[h]	kJ mol^{-1}	E_a
Andrade exponent	0.2 – 0.4[i]	–	α
Surface temperature	90 – 106[jk]	K	$T_{\rm surf}$

[a] Petricca et al. (2023).
[b] Howell (2021).
[c] Wahr et al. (2006).
[d] Cole and Durell (1995).
[e] Běhounková et al. (2021).
[f] Hussmann et al. (2002).
[g] Hussmann et al. (2002).
[h] Goldsby and Kohlstedt (2001).
[i] Castillo-Rogez et al. (2011).
[j] Spencer et al. (1999).
[k] Ashkenazy (2019).

2.2.2. Viscoelastic deformation modeling

Accounting for two different layers within the ice shell allows us to model the stagnant lid regime that develops in layers with highly temperature-dependent viscosity, such as ice I. As the temperature increases from about 100 K at the surface to the melting point at the ice–ocean interface, in the range 250 – 270 K, the viscosity decreases by several orders of magnitude. If the shell is thick enough, this viscosity contrast can trigger solid-state convection (McKinnon, 1999; Pappalardo et al., 1998), which becomes the main heat transfer mechanism in the lower shell. The upper layer is cold and transfers heat by thermal conduction. The properties of the convective layer, where a significant amount of tidal heating is generated, considerably affect the calculation of the tidal Love numbers. In our parameter space (Table 2), we included the rheological properties of Europa's interior layers, which are relevant to modeling the viscosity structure of the ice shell. These parameters are randomly varied along with the radial and density structures and then used to compute the Love numbers only for the models that are consistent with the measured mass and MoI.

The treatment of convection in the ice shell is carried out by modeling the thermal and viscosity structures of the layer with scaling laws (Solomatov, 1995) in a 1-dimensional domain. This approach allows us to reduce the computational effort required to compute a large number of models in the Monte Carlo algorithm and has been successfully applied to past investigations of the outer shells of icy satellites (*e.g.,* Hussmann et al., 2002; Deschamps and Sotin, 2001). The thermal structure of the ice layer is computed by starting from the bottom, where the temperature is given by the melting point of the ice Ih–water phase diagram. We approximate the melting curve of ice Ih with the Simon–Glatzel equation given by Choukroun and Grasset (2007):

$$T_m = T_0 \left(\frac{P_m - P_0}{a} + 1 \right)^{\frac{1}{c}} \tag{6}$$

where the empirical parameters $a = -414.5$ MPa and $c = 8.38$ and the reference pressure $P_0 = 6.11657 \times 10^{-4}$ MPa and temperature $T_0 = 273.15$ K are fit to experimental data (Choukroun and Grasset, 2007). The melting pressure P_m is derived from the density and total thickness of the ice layer through hydrostatic equilibrium. The convective portion is assumed to be isothermal and its temperature is derived using the approximation given by Howell (2021):

$$T_{\text{conv}} = \frac{\sqrt{4T_m R/E_a + 1} - 1}{2R/E_a} \tag{7}$$

where R is the gas constant and E_a is the creep activation energy, which depends on the dominant deformation mechanism. Since this parameter is not well constrained, we include it in our parameter space and randomly vary it in the range $50 - 70\,\text{kJ mol}^{-1}$. To compute the rheological structure of this layer, we assume that the ice behavior is described by diffusion creep and the viscosity is given by an Arrhenius equation (*e.g.,* Goldsby and Kohlstedt, 2001):

$$\eta_{\text{conv}} = \eta_0 \exp\left[\frac{E_a}{RT_m} \left(\frac{T_m}{T_{\text{conv}}} - 1 \right) \right] \tag{8}$$

where the ice melting point viscosity η_0 is randomly varied in the range $10^{12} - 10^{16}$ Pa s. The computed viscosity and ice thickness are then used to evaluate whether the lower ice layer is in the subsolidus convection regime. The Rayleigh number of this layer is:

$$Ra_{\text{conv}} = \frac{\alpha_{\text{ice}} \rho_{\text{ice}} g (T_m - T_{\text{surf}}) d_{\text{ice}}^3}{\eta_{\text{conv}} D_{\text{ice}}} \tag{9}$$

where $\alpha_{\text{ice}} = 1.6 \times 10^{-4}$ K^{-1} is the ice thermal expansivity, g is the gravitational acceleration, T_{surf} is the surface temperature, $d_{\text{ice,conv}}$ is the thickness of the convective layer, and $D_{\text{ice}} = 1.4 \times 10^{-6}$ m^2 s^{-1} is the ice thermal diffusivity. The critical Rayleigh number determines the onset of convection (Solomatov, 1995):

$$Ra_{\text{crit}} = 20.9 \left(\frac{E_a (T_m - T_{\text{surf}})}{RT_{\text{conv}}^2} \right)^4 \tag{10}$$

If $Ra_{\text{conv}} > Ra_{\text{crit}}$, the ice shell is unstable against convection. In this case, the tidal deformations of the lower layer are modeled with an Andrade rheology, with the Andrade exponent randomly varied between 0.2 and 0.4 (Table 2). The cold upper layer is assumed to deform elastically. The shear modulus is equal in the two layers and is assigned by Monte Carlo sampling within the range 2.5 – 4.5 GPa. In the opposite case of $Ra_{\text{conv}} < Ra_{\text{crit}}$, the whole ice shell is assigned a high viscosity and responds elastically to tidal deformations.

Viscoelastic and anelastic deformations may also occur in Europa's deep interior, depending on the temperature and rheological structures, which are not well determined. Therefore, tidal dissipation in the deep interior is largely unconstrained, and some previous studies on the thermal state of Europa assumed that the deep interior tidal response is elastic (*i.e.,*non-dissipative; Ojakangas and Stevenson, 1989; Hussmann et al., 2002; Moore, 2006; Ruiz, 2005). Běhounková et al. (2021) investigated the effects of tidal heating on the thermal history and melt production of Europa using a 3D model and the rheology of the deep interior described by the Andrade model and the temperature-dependent viscosity. Here, we adopt a simple model of the deep interior response based on the Andrade rheology, an average viscosity varied between that at the melting point of the rocks ($\sim 10^{18}$ Pa s,Běhounková et al., 2021) and a value representative of a cold, elastic interior (10^{22} Pa s). The shear modulus is randomly drawn uniformly from the range 50 – 70 GPa.

2.2.3. Pressure-induced density increase with depth across the ocean

We investigate the effects of density variations with depth across the ocean on tidal deformations for Europa, Ganymede, and Callisto using *PlanetProfile* to self-consistently model the effects of pressure on ocean density. Mitri et al. (2014) showed that the water density gradient driven by pressure is relevant for the computation of tidal Love numbers of ocean worlds, with Titan's k_2 increasing by about 3 – 4% when compared to the case of uniform density throughout the ocean. This difference might be greater than the measurement uncertainty that will be achieved by future missions at ocean worlds (*e.g.,* Europa Clipper and JUICE); therefore, quantifying these effects for the Galilean moons will be beneficial for future investigations.

PlanetProfile computes the ocean density by assuming that the ocean is characterized by an adiabatic thermal profile:

$$\frac{\partial T}{\partial P} = \frac{\alpha_{\text{ocean}} T}{\rho C_P} \tag{11}$$

where T is the temperature, P is the pressure, α_{ocean} is the fluid thermal expansivity, C_P is the specific heat, and all quantities in (11) are depth-dependent. Starting from the temperature (input into the software) and the pressure at the bottom of the ice shell, the ocean profiles are calculated using relevant equations of state (EoS) for pure water (through SeaFreeze; Journaux et al., 2020), seawater (Gibbs seawater package; McDougall and Barker, 2011) and $MgSO_4$ (Vance and Brown, 2013; Vance et al., 2014), which account for the dependence of pressure and temperature of α_{ocean}, ρ, and C_P. To calculate the pressure profile, a linear pressure step ΔP is set as input that defines the resolution of the ocean profiles. The physical properties are propagated to the bottom of the ocean, corresponding to the ocean–rock interface or to the phase transition to high-pressure ice phases for the larger moons. We assess the influence of variations with depth in the density of the ocean for the three moons by separately examining each of the different compositions available in *PlanetProfile*.

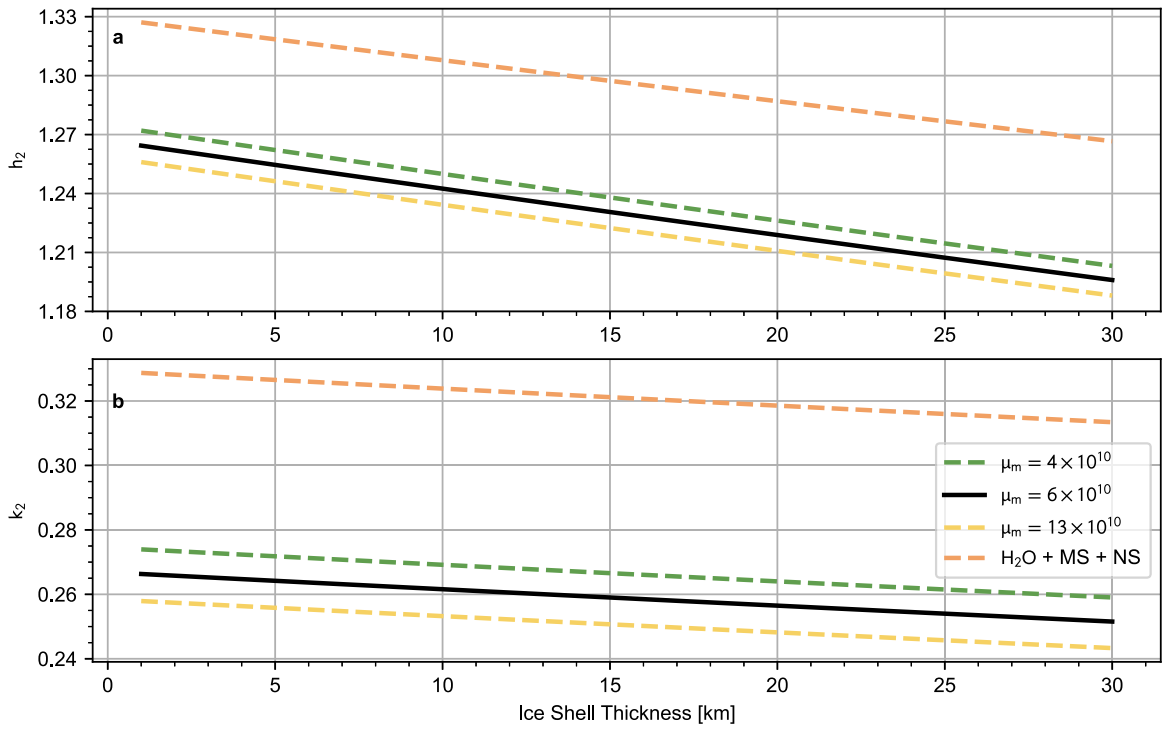

Fig. 1. Love numbers (a) h_2 and (b) k_2 computed with PyALMA^3 for varying ice shell thickness and mantle rigidity. We adopted the modeling by Wahr et al. (2006) to compare our results with the tidal Love numbers they computed (Figure 1 in Wahr et al., 2006). The H_2O + MS + NS case is based on a hydrosphere composed of the eutectic system H_2O-$MgSO_4$-Na_2SO_4 (Kargel et al., 2000).

3. Results

3.1. Benchmark and validation

We validated PyALMA^3 by comparing the predicted tidal response for Europa with previous studies. Our results are provided in terms of the real parts of the tidal Love numbers, which are indicated by k_2, h_2, l_2 throughout the paper. Wahr et al. (2006) computed the tidal Love numbers of Europa using a compressible elastic framework to investigate the possibility of inferring the ice thickness from measurements of k_2, h_2, or a combination of the two. They concluded that although recovery of the thickness of the ice shell through observations of only k_2 or h_2 can be significantly biased from other relevant parameters such as the rock shear modulus or the ocean density, the gravimetric factor $\delta_g = 1+k_2-h_2$ is more robust to these uncertainties and its measurement is useful for investigating the structure of the ice shell. We adopted the same interior modeling as used by Wahr et al. (2006), except for our assumption of incompressibility. Thus, the density of ice and the density of the ocean are assumed to be $920\,\mathrm{kg\,m^{-3}}$ and $1000\,\mathrm{kg\,m^{-3}}$, respectively. The density of the metallic core is given by the density of the eutectic mixture in the Fe-FeS system ($5150\,\mathrm{kg\,m^{-3}}$). The density and size of the rocky mantle are derived from the radius of the body and the total mass. The ice shear modulus is assumed to be equal to 2 GPa. As in the reference work, we use different values of the mantle shear modulus (*i.e.,* 40 GPa, green dashed line in Fig. 1; 60 GPa, black solid line; 130 GPa, yellow dashed line). Another case we reproduced from Wahr et al. (2006) shows the tidal Love numbers obtained by assuming that the hydrosphere is composed of the eutectic system H_2O-$MgSO_4$-Na_2SO_4 based on Kargel et al. (2000) (ice and ocean density equal to $1144\,\mathrm{kg\,m^{-3}}$ and $1208\,\mathrm{kg\,m^{-3}}$, respectively, orange dashed line). For each case, we compute the corresponding k_2 and h_2 as a function of ice thickness, reported in Fig. 1. Although our modeling assumes an incompressible behavior, the results show substantial agreement with the results of Wahr et al. (2006) in their Fig. 1. A more rigorous assessment of the effects of assuming incompressibility is presented in Section B.

We also compared the output of PyALMA^3 with the output of ALMA^3 obtained for the same interior modeling (Figure S1) to validate the conversion to Python. Relative differences between the tidal Love numbers are negligible, on the order of 10^{-14} for h_2 and 10^{-15} for k_2.

3.2. Tidal response of Europa

This section shows the results of the exploration of Europa's tidal response carried out with the Monte Carlo sampler. Techniques based on the exploration of a large parameter space combined with the generation of a broad number of models allow for a robust assessment of geophysical quantities that describe the interior structure of a body. This robustness is ensured by the wide range of combinations between the interior properties sampled by the Monte Carlo algorithm, which account for all the uncertainties associated with the quantities relevant to the determination of the geophysical parameters. Here, we provide the tidal Love numbers resulting from the application of PyALMA^3 to our large-scale modeling. These predictions can be useful for future investigations and simulations of Europa's interior.

Fig. 2 shows the distribution of the real parts of the Love numbers k_2, h_2 and l_2 computed at Europa's orbital period (85.2 h). Although these distributions depend on the assumptions and the specific modeling of Europa's interior that we adopted, the broad parameter space we have explored suggests that it is likely that Europa's Love numbers fall in the ranges given by $k_2 = 0.24 \pm 0.03$, $h_2 = 1.05 \pm 0.11$ and $l_2 = 0.27 \pm 0.03$, accounting for 3-sigma intervals.

With the resulting models, we analyze the influence of each interior property on the tidal Love numbers to better understand which parameters are most relevant in determining the tidal response. Although the sensitivity of the Love numbers to the interior properties of ocean worlds is generally understood qualitatively, rigorous analyses have not been performed for most of these bodies, with the notable exception of the study by Kamata et al. (2016), which used the method of variation

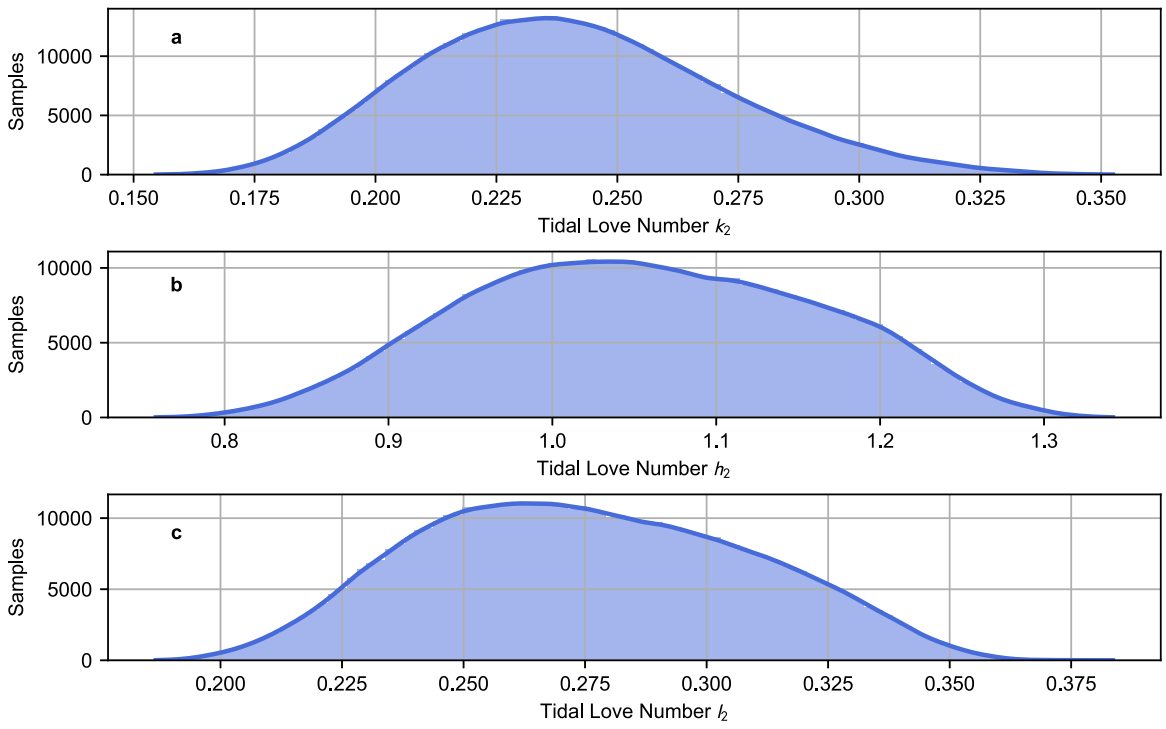

Fig. 2. Histograms of Europa's tidal Love numbers obtained with our Monte Carlo sampling. The resulting distributions can be summarized as: (a) $k_2 = 0.24 \pm 0.03$, (b) $h_2 = 1.05 \pm 0.11$, (c) $l_2 = 0.27 \pm 0.03$.

in partial means to investigate the tidal response of Ganymede. Our interior modeling based on Monte Carlo sampling also allows us to use statistical techniques to study this sensitivity. We perform our analysis by computing the Spearman correlation between the tidal Love numbers and the interior parameters, which tests for any monotonic relationship between the quantities considered (Spearman, 1904). A correlation of 1 indicates that an increase in the parameter considered always leads to an increase in the Love numbers, while a correlation of -1 implies that the Love numbers become smaller when the parameter increases. The statistical significance of the correlation is tested with its p-value. Fig. 3 shows the correlations among the real parts of the tidal Love numbers k_2 and h_2, their imaginary parts k_{2i} and h_{2i}, and the interior properties that determine our model. The l_2 Love number and its imaginary part are not shown since their correlations with the other quantities are very close to the corresponding values obtained for h_2.

The strong anti-correlations between the core density and radius and the one between ice and ocean thicknesses arise from the constraint given by the MoI. In fact, these properties trade off to determine the MoI, implying that a measurement of this quantity cannot separately constrain the core density and size or the ice and ocean thicknesses. This ambiguity is very well known from previous works on the inversion of Europa's interior (*e.g.,* Petricca et al., 2023), but Fig. 3 provides a quantification of this non-uniqueness of the inversion solution. The correlations of the interior properties with the tidal Love numbers are also interesting. The parameters that influence mainly k_2 are the ice thickness, the depth of the ocean, and the density of the ocean. This implies that a measurement of k_2 cannot unambiguously constrain one of these quantities, as shown in previous work (*e.g.,* Wahr et al., 2006). Since the MoI imposes a constraint on hydrosphere thickness, ice and ocean thicknesses are strongly anticorrelated, and therefore static gravity provides an additional constraint to remove some degree of ambiguity. However, the substantial dependence of k_2 on the density of the ocean introduces additional uncertainty. The sensitivity of h_2 to interior properties is similar, with the exception of its weak correlation with ocean density. This lack of dependence of h_2 on ocean density implies that if viscoelastic and anelastic deformations are neglected, measurements of the static gravity field (*i.e.,* mass and MoI) combined with k_2 and h_2 could separate the effects of ocean density from ice and ocean thicknesses. Therefore, the estimation of the factor $\delta_g = 1+k_2-h_2$ was suggested as a more robust way to infer the thickness of the ice layer by Wahr et al. (2006), although some uncertainty would still be introduced by the ice shear modulus. This is evident in Fig. 3 because the tidal gravimetric factor δ_g does not show any correlation with the ocean density. Although one would expect that increasing k_2 would result in an increase of δ_g (*i.e.,*positive correlation), this is actually not the case, as they are anti-correlated. This is due to the large correlation between k_2 and h_2. Therefore, increasing k_2 always results in an increase of h_2, which is more strongly anti-correlated with δ_g than k_2, ultimately leading to a decrease of the gravimetric factor. It should be noted that the tidal Love numbers were calculated by Wahr et al. (2006) assuming an elastic tidal response. When including viscoelastic and anelastic deformations in the ice layer, the uncertainties in determining the thickness of the ice from measurement of the tidal gravimetric factor $1+k_2-h_2$ increase greatly. Thus, neglecting the anelasticity of the ice shell can significantly bias the estimation of the ice thickness from observation of the $1+k_2-h_2$ factor. Fig. 3 also shows that the properties of the deep interior only have a small effect on the determination of the Love numbers, because the properties of the outer layers dominate the tidal response. This finding is consistent with the results presented by Kamata et al. (2016) on Ganymede and it indicates that the Love numbers will not be useful in inferring the properties of the deep interior of Europa. On the other hand, this small sensitivity implies that the properties of the deep interior will not bias the recovery of the characteristics of the outer layers. Other significant correlations occur between the imaginary parts of the Love numbers and the rheological properties of the ice shell that determine its viscosity. This behavior is connected to the expectation that most of the tidal dissipation at Europa, described by the imaginary parts of the tidal Love numbers, occurs in the warm convective portion of the ice shell.

These considerations are better illustrated in Figs. 4–6, where we show k_2, h_2, and the tidal gravimetric factor, respectively, calculated

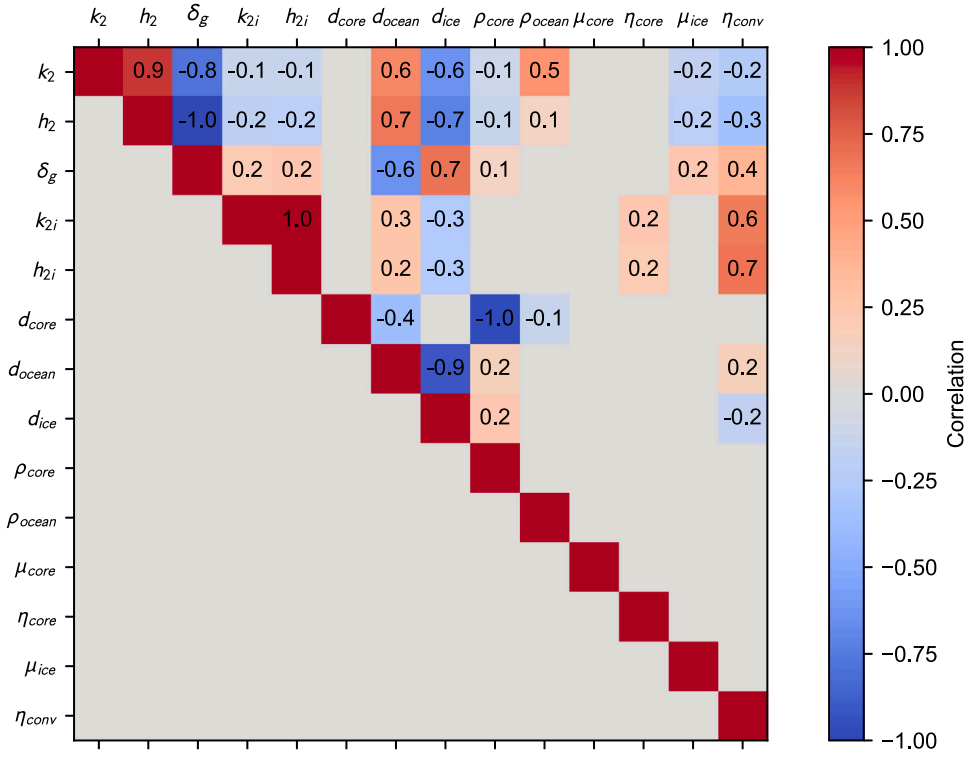

Fig. 3. Spearman's correlation index between the complex tidal Love numbers and the interior properties that we consider. Only correlations with magnitude larger than 0.1 are shown. The tidal Love numbers are mostly affected by the properties of the outer layers, especially the ice and ocean thicknesses, and the ocean density. Some correlations such as those between the core density and size arise from the imposed MoI constraint.

with the models resulting from our Monte Carlo simulation. The gray shaded areas represent the projected uncertainty in the determination of these geophysical quantities with Europa Clipper (Mazarico et al., 2023; Steinbrügge et al., 2018). The uncertainty in h_2 is based on simulations by Steinbrügge et al. (2018), who showed that it can range between 0.04 and 0.17, depending on the performance of the crossover investigation. In all three figures, panels a and b show models with fully conductive shells (*i.e.*, $Ra_{\text{conv}} < Ra_{\text{crit}}$) that deform elastically, while panel c shows models for which the ice layer is unstable against convection (*i.e.*, $Ra_{\text{conv}} > Ra_{\text{crit}}$). Focusing on elastic shells only, the large influence of ocean density on k_2 is evident (Fig. 4a) with variations of approximately 40% between end members ($1000 - 1300\,\text{kg m}^{-3}$), while the sensitivity of h_2 on the same quantity is smaller (Fig. 5a, differences of $5 - 15\%$). A simple linear regression shows that an increase in the ocean density of $10\,\text{kg m}^{-3}$ increases the corresponding k_2 by 0.0020 and h_2 by 0.0016. Similarly, if the ice thickness increases by 10 km, k_2 and h_2 decrease by 0.006 and 0.023, respectively. For the ice shear modulus, the conclusion is the opposite, with h_2 showing a greater dependence. As the thickness of the ice shell increases (> 50 km), the value of h_2 is determined solely by the thickness of the ice and the shear modulus. The different sensitivities of the tidal parameters are combined when considering the factor $1 + k_2 - h_2$, for which the influence of the ocean density is reduced compared to independent measurements of k_2 or h_2 (Fig. 6a). The ice shear modulus has a larger influence and its uncertainty can bias the recovery of the ice thickness, especially for thick shells (Fig. 6b).

In addition to these uncertainties, which have already been investigated and accounted for in previous studies, we show that the viscoelastic response of the shell to the tidal forcing represents a relevant source of uncertainty in the determination of the ice thickness. Figs. 4c, 5c, and 6c show the values of k_2, h_2 and $1 + k_2 - h_2$, respectively, for models that include ice shells unstable to convection. In the convective portion of the shell, tidal deformations can be enhanced if the viscosity of the ice is low, significantly affecting the resulting Love numbers. The absolute values of k_2 and h_2 increase and the corresponding value $1 + k_2 - h_2$ decreases. This significantly widens the space of solutions, and the interpretation of future measurements will require careful modeling and evaluation of the viscoelastic effects.

3.3. Effects of liquid density gradient in the ocean

The liquid density in the subsurface oceans is expected to increase with depth due to the self-compression of water. Because the density of the ocean is a key parameter in determining the tidal responses of ocean worlds, these pressure-induced variations in the water density can significantly affect the tidal Love numbers. We computed the tidal Love numbers for Europa, Ganymede, and Callisto by integrating `PyALMA`[3] with *PlanetProfile* to investigate the effects of the density gradient across the ocean on their tidal responses. For both Europa and Callisto, we consider a pure-water ocean, $MgSO_4$ with a salt concentration equal to 100 g/kg, and a seawater composition with Earth's mean salt concentration (34 g/kg). For pressures greater than 200 MPa, the EoS for the seawater ocean becomes unstable and thus is not applicable to larger bodies such as Ganymede. Therefore, we evaluate the self-compression effects of an ocean that includes 10 g/kg of $MgSO_4$ as an intermediate case. Interior models generated by *PlanetProfile* include the radial structures of the density and the shear and bulk moduli of each layer needed to calculate the tidal deformations. The latter is ignored by `PyALMA`[3] in evaluating the Love numbers due to the incompressibility approximation. Some of the density and shear modulus profiles generated by *PlanetProfile* are shown in Figures S2–S4.

The effects of the density gradient are assessed by evaluating the difference Δk_2 between the Love number calculated with the full radial profile and the corresponding value computed with the ocean density averaged over the ocean depth. Fig. 7 shows Δk_2 for Europa (Fig. 7a), Ganymede (Fig. 7b), and Callisto (Fig. 7c). For all moons, the effect is of the order of a few percent of the k_2 value, consistent with previous estimates for Titan (Mitri et al., 2014). In terms of absolute value, the

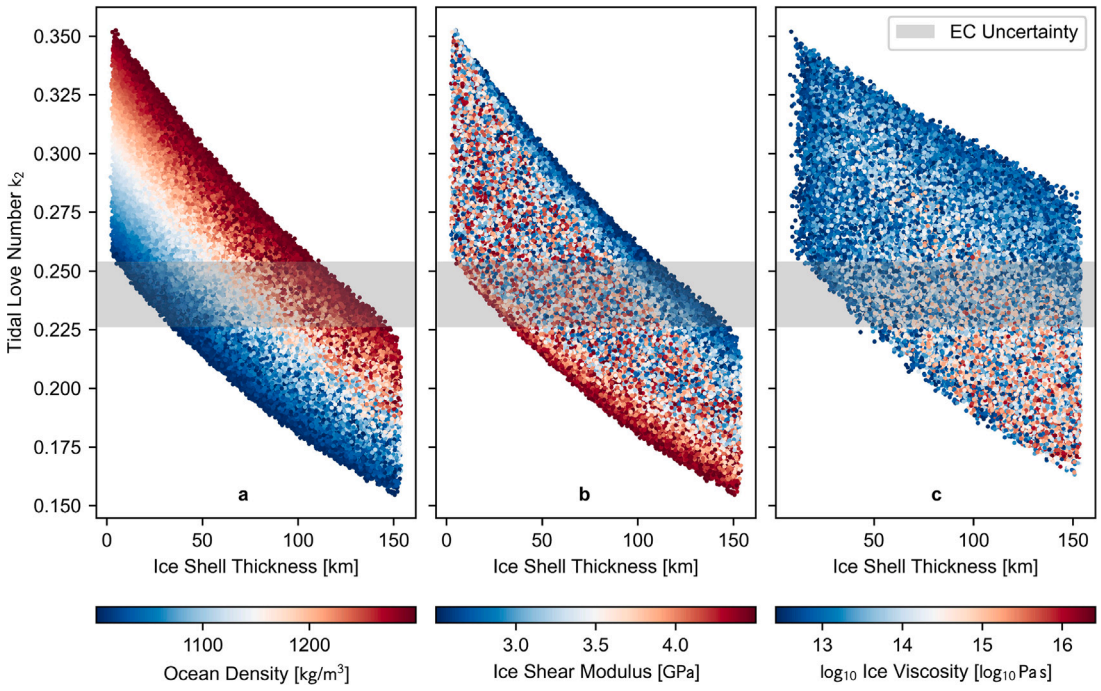

Fig. 4. Tidal Love number k_2 as a function of varying ice shell thickness for models including an elastic (a, b) and (c) viscoelastic ice layer. The clear vertical separation between values of k_2 in panel (a) shows the large influence of the ocean density. In contrast, the ice layer rheological properties have a smaller influence (b, c). The inclusion of viscoelastic deformations (c) widens the parameter space and increases the absolute value of k_2. Gray shaded areas represent the projected uncertainties from Europa Clipper Gravity/Radio Science investigation (Mazarico et al., 2023).

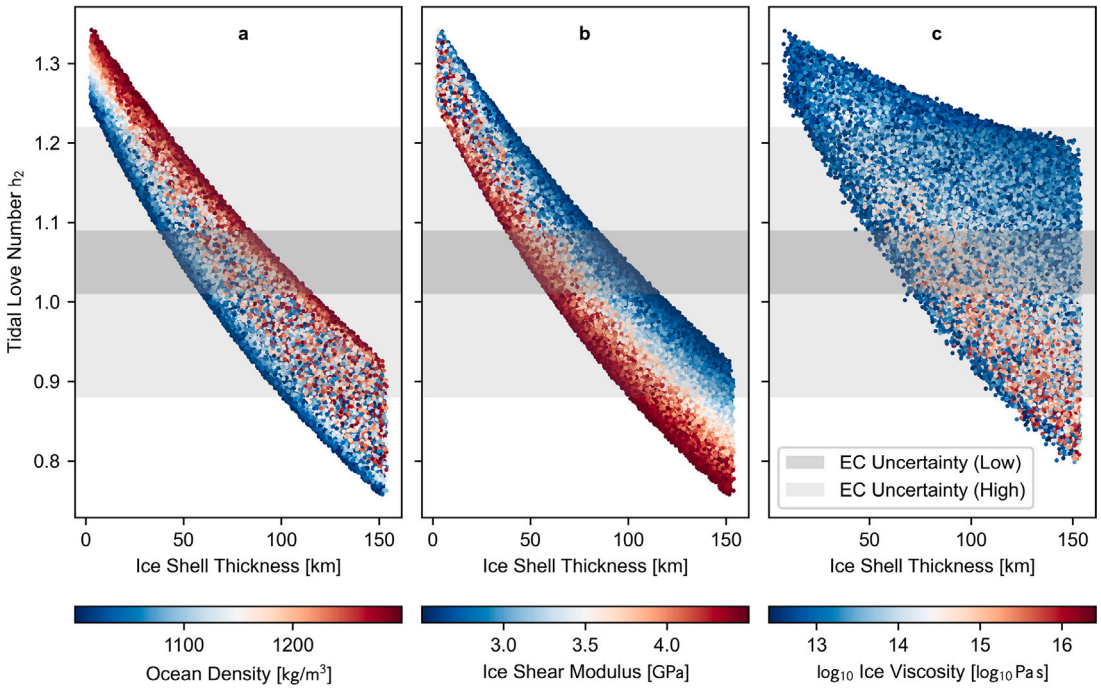

Fig. 5. Tidal Love number h_2 as a function of varying ice shell thickness for models including an elastic (a, b) and (c) viscoelastic ice layer. In contrast to k_2, h_2 is more sensitive on the ice shear rigidity than on the ocean the density. Gray shaded areas represent the projected uncertainties from Europa Clipper data in two different scenarios (Steinbrügge et al., 2018).

errors introduced if density variation with depth is not taken into account are approximately 0.005, 0.015, and 0.013 for Europa, Ganymede, and Callisto, respectively. For Europa and Callisto, the errors increase for deeper oceans considering the range of ocean depth consistent with the MoI and EoS constraints introduced by *PlanetProfile*. However, this trend should not be extrapolated to larger ocean depths, as illustrated in the Ganymede case. In the latter case, when deep oceans are considered (> 300 km), the errors decrease with increasing depth, showing that the ability of an average density to describe the ocean tidal response improves with increasing depth.

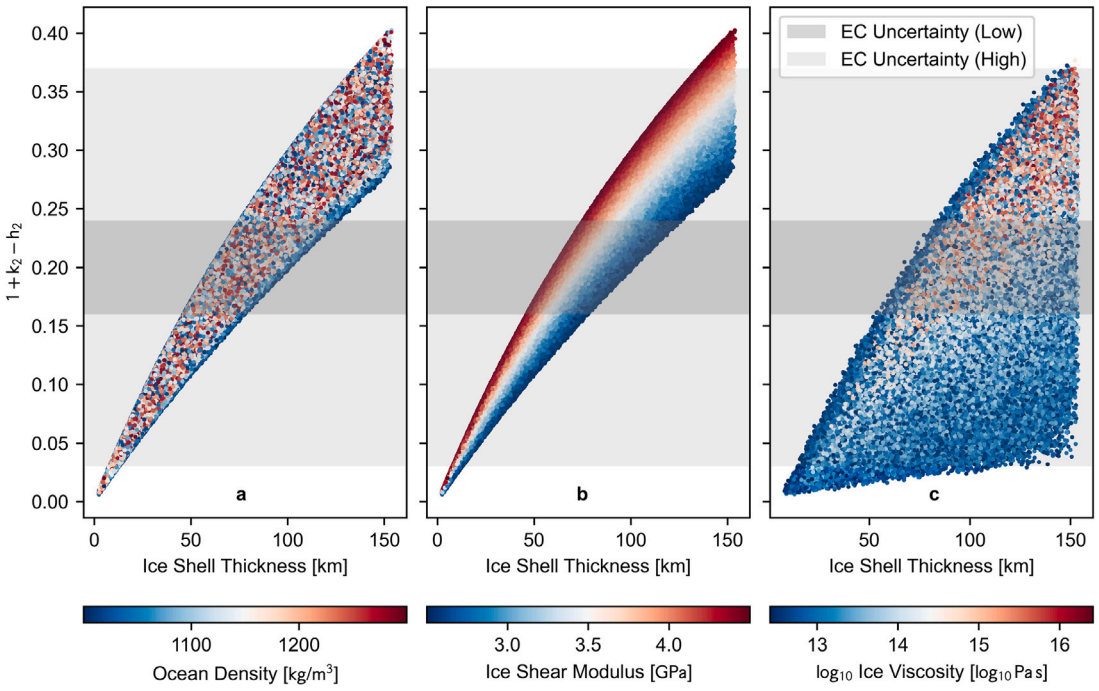

Fig. 6. Tidal gravimetric factor $1+k_2-h_2$ as a function of varying ice shell thickness for models including an elastic (a, b) and (c) viscoelastic ice layer. The determination of this factor can provide a good estimate of the ice thickness if this is low and elastic modeling is assumed. However, the inclusion of viscoelastic effects significantly reduces the utility of the gravimetric factor in resolving the ice thickness (c). Gray shaded areas represent the projected uncertainties from Europa Clipper data in two different scenarios (Steinbrügge et al., 2018; Mazarico et al., 2023).

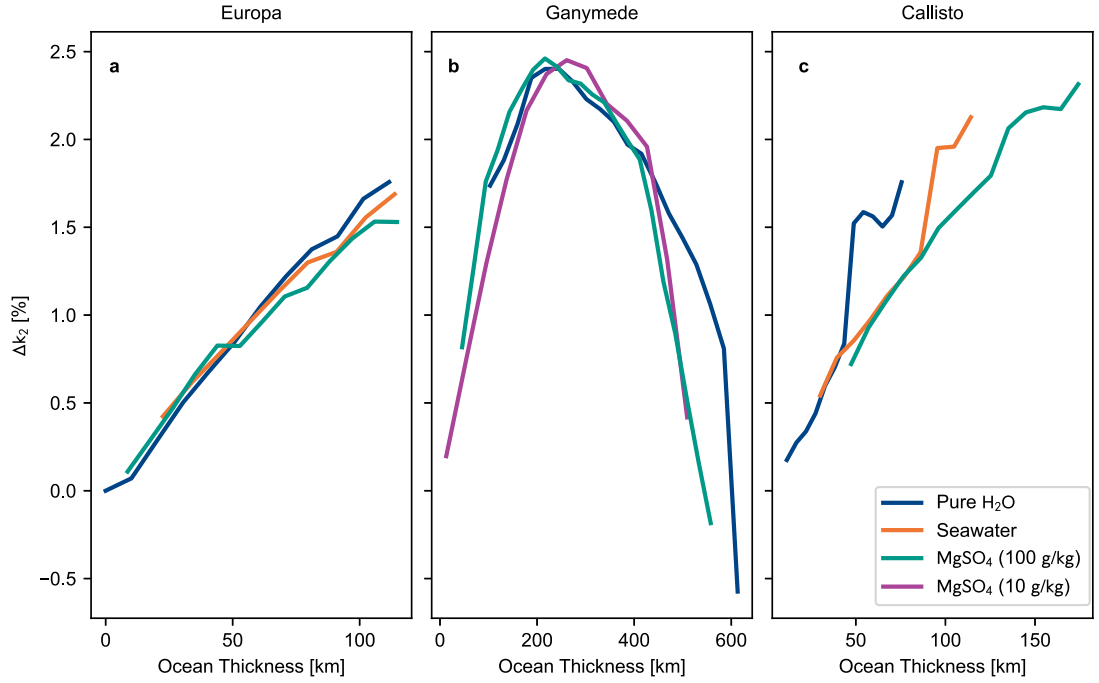

Fig. 7. Effects of variations of the water density across the ocean on the tidal Love number k_2 for (a) Europa ($\sim 1.7\,\%$ or ~ 0.005), (b) Ganymede ($\sim 2.5\,\%$ or ~ 0.015) and (c) Callisto ($\sim 2.3\,\%$ or ~ 0.013).

These results were examined against the same interior models using a numerical toolbox to calculate the Love numbers developed for the case of both rocky (Bagheri et al., 2019; Dmitrovskii et al., 2022), and icy bodies (Bagheri et al., 2022b). This toolbox uses the spectral element method to compute the complex Love numbers of a compressible body exploiting different viscoelastic models such as Maxwell, Extended Burgers, Andrade, and Sundberg–Cooper. Despite the different methods used by the code (*i.e.*,compressible model, in contrast to the assumption of incompressibility in PyALMA^3), we find that the effects of the density gradient in the ocean are consistent with

those evaluated by using PyALMA^3 (*e.g.,* differences between the two codes of approximately 3×10^{-5} for the deepest ocean in the case of Europa).

4. Discussion

The analyses carried out here will be valuable for future investigations of the interiors of icy bodies by measuring their tidal responses. Europa Clipper and JUICE are set to explore the Jupiter system in the next decade, providing radio science data from which the gravity field and the tidal response of Europa, Ganymede, and Callisto will be measured. The Europa Clipper Gravity and Radio Science investigation will measure the tidal Love number k_2 of Europa with an accuracy of $1.4\times10^{-2} - 1.8\times10^{-2}$ (Mazarico et al., 2023), while the 3GM experiment onboard JUICE is expected to yield Ganymede and Callisto k_2 to better than 10^{-4} and 5.9×10^{-2}, respectively (Cappuccio et al., 2020, 2022). For all moons, the determination of the ice shell thickness and ocean depth will be challenged by the effects of viscoelastic deformations because the Love numbers and their combination are sensitive to the thermal and viscosity structure of the ice layer. Especially in the case of Europa, it is likely that measurements of the tidal deformations alone will not enable the determination of the hydrosphere properties. As shown in Figs. 4–6, the projected uncertainties in determining Europa's tidal Love numbers could be too large to allow accurate retrieval of the thickness of the ice shell and the depth and density of the ocean. The recovery of hydrosphere properties will then be significantly improved through the combination of gravity and tidal observations with other datasets, such as magnetic induction measurements (Vance et al., 2021; Petricca et al., 2023; Roberts et al., 2023). Petricca et al. (2023) developed a methodology to combine gravity and magnetic field measurements to improve the characterization of the hydrospheres of icy moons. They showed that simultaneously enforcing the constraints given by static gravity (*i.e.,* mass and MoI) and magnetic induction measurements provides a robust way to infer the ice thickness and ocean depth. The inclusion of tidal Love numbers among the constraints will narrow down the ocean density and salinity, yielding a comprehensive characterization of the subsurface ocean. Additional constraints can be determined by radar sounding, which could provide the thickness of the ice shell or the thickness of the outer cold lid if the attenuation induced by the lower warm ice layer is strong (*e.g.,* Roberts et al., 2023).

An efficient technique that produces interior models consistent with multiple geophysical observations by combining different datasets relies on the Markov chain Monte Carlo (MCMC) algorithm (*e.g.,* Petricca et al., 2023; Genova et al., 2019). The difference from the simpler approach proposed here is that the MCMC method requires defining a probability distribution for the observations that constrains the inverse problem (*e.g.,* the MoI used here). For example, previous work on Europa's interior inversion assumed a Gaussian distribution for the MoI (Petricca et al., 2023), with the mean given by the observed value and the standard deviation given by the measurement uncertainty, while here we assume that the MoI is uniformly distributed in the $3 - \sigma$ range. The MCMC method leads to a more efficient sampling of the parameter space that is suitable for the Bayesian inversion of the interior structure from observations. Within a Bayesian framework, the focus is on sampling the most probable regions of the parameter space. Since the goal of this work is to explore the parameter space and the sensitivity of the Love numbers on the interior properties without providing any constraint on them, we adopted a simpler approach that does not require generating Markov chains. In this way, we were able to simply explore the parameter space of acceptable models as defined by the data and our prior constraints (Table 2). The successful application of the MCMC algorithm requires generating a large number of interior models, on the order of a few to tens or hundreds of millions, depending on the specific application, to converge to the final probability distributions for the parameters and observations. Thanks to the efficient numerical scheme enabled by the propagator matrix technique, PyALMA^3 will be suitable for use in these multidisciplinary investigations.

An additional aspect that should be taken into account in future investigations is ocean modeling. We showed that the effects of the radial density gradient in the ocean could induce variations in k_2 that could be large, potentially biasing the estimation of interior properties from measurements of the tidal response. Taking into account the predicted accuracy in the determination of Europa's k_2 from Europa Clipper data, the effects of water density gradient might be below the noise threshold. This is not the case for Ganymede, for which these effects might be two orders of magnitude larger than the high precision predicted for the 3GM experiment onboard JUICE. For both moons, accurate modeling of the ocean properties will be essential to interpreting future tidal observations, and new experimental data to derive equations of state for relevant compositions, pressures, and temperatures will be important in this context.

5. Summary

In this manuscript we presented PyALMA^3, a Python framework based on ALMA^3 dedicated to modeling the planetary response to tidal deformations. We validated PyALMA^3 by applying it to Jupiter's moon Europa and comparing our results with previous investigations of the satellite's tidal response. We combined this benchmark of the software with a simple Monte Carlo technique used to explore the tidal deformations of Europa, which allowed us to more rigorously assess the effects of the interior properties on the tidal Love numbers. We demonstrated that the tidal response of Europa is significantly affected by the properties of the outer layers, especially the ice and ocean thicknesses, and the ocean density. In contrast, our results indicate that the properties of the deep interior have negligible effects on the tidal deformations. Furthermore, we showed that the rheological response due to the viscosity of the ice shell also plays a key role in determining the tidal Love numbers, negatively affecting the recovery of the outer layer properties from a combined measurement of k_2 and h_2, which has been the subject of several geophysical studies of ocean worlds. Given the large number of parameters that determine the response to tides, a combination of different types of measurement will be fundamental to achieving an accurate characterization of icy moon interiors, and PyALMA^3 provides a means to relate some of these critical measurements. Finally, our results show that accounting for the pressure-induced variations of water density in the ocean is critical for a correct interpretation of future measurements of the tidal responses of ocean worlds. In fact, this effect (on the order of 2–3 % on the tidal Love number k_2 of the Galilean moons) is close to the projected measurement uncertainty in the determination of Europa's tidal Love number from Europa Clipper's radio science data and, most importantly, two orders of magnitude larger the expected accuracy of the 3GM experiment onboard JUICE.

CRediT authorship contribution statement

Flavio Petricca: Writing – original draft, Validation, Methodology, Investigation, Conceptualization. **Saikiran Tharimena:** Writing – review & editing, Validation, Software. **Daniele Melini:** Writing – review & editing, Validation, Software, Conceptualization. **Giorgio Spada:** Writing – review & editing, Conceptualization. **Amirhossein Bagheri:** Writing – review & editing, Validation, Formal analysis. **Marshall J. Styczinski:** Writing – review & editing, Software, Data curation. **Steven D. Vance:** Writing – review & editing, Project administration, Conceptualization.

Declaration of competing interest

The authors declare that they have no known competing financial interests or personal relationships that could have appeared to influence the work reported in this paper.

Data availability

No data was used for this research. The code PyALMA^3 has been released to accompany this manuscript.

Acknowledgments

The data in this work were generated by the open-source frameworks PyALMA^3 (Styczinski et al., 2024) and *PlanetProfile* (Styczinski et al., 2023b). FP acknowledges funding from the Italian Space Agency (ASI) under contract 2021-19-HH.0. Parts of this work were carried out at the Jet Propulsion Laboratory, California Institute of Technology, under a contract with NASA (80NM0018D0004), with support from NASA's Habitable Worlds program (16-HW16 2-0065), the NASA Astrobiology Institute Hydrocarbon Worlds project (17-NAI8-0017), and from NASA's Precursor Science Investigations for Europa (22-PSIE22_2-0024). GS is funded by a RFO grant of DIFA. MJS was supported by an appointment to the NASA Postdoctoral Program at the Jet Propulsion Laboratory, California Institute of Technology, administered by Oak Ridge Associated Universities under a contract with NASA (80HQTR21CA005). AB acknowledges the support from SNSF by grant number P500PT_214435. The authors acknowledge that parts of this work have been carried out on the traditional lands of the Western Shoshone, Northern and Southern Paiute, Washoe, and Tongva peoples.

Appendix A. Computation of Love Numbers

The problem of computing the deformations of a solid body subject to self-gravitation has traditionally been approached by assuming that the body is spherically symmetric. The equilibrium equations are usually solved using two different classes of methodologies.

Direct numerical integration schemes do not require additional assumptions and are based on the original formulation developed to calculate the elastic deformations associated with seismic waves (Alterman et al., 1959; Takeuchi and Saito, 1972). This formalism was extended to modeling viscoelastic deformations through the correspondence principle, according to which the Fourier (or Laplace) transform of the equilibrium equations can be cast as a formally elastic problem if frequency-dependent shear and bulk moduli are defined. This approach can be used to model deformations induced by any periodic forcing, such as those due to tidal and loading potentials (Tobie et al., 2005; Michel and Boy, 2021). One of the main drawbacks of this method is the numerical instability arising from the presence of a fluid layer in the body, as with subsurface oceans. To solve this problem, previous work introduced the additional assumption of static tides (*e.g.,* Wahr et al., 2006; Mitri et al., 2014).

Another class of methods used to compute the Love numbers of planetary bodies is the propagator matrix method (Peltier, 1974; Sabadini et al., 1982), originally developed with the assumption that bulk deformations can be neglected, *i.e.,* the only effects accounted for are deviatoric stresses and strains related to shear rigidity and viscosity. The body is modeled with incompressible layers with uniform properties. This approach is less computationally expensive because, in the incompressible limit, analytical expressions for the propagator in each layer are available, and hence no numerical integration is needed. Compared to numerical integration schemes, it has the advantage of being stable when layers with a vanishing shear modulus (*i.e.,* behaving as fluids) are encountered. These characteristics made this method suitable for planetary applications, particularly for the interior modeling of ocean worlds (*e.g.,* Moore and Schubert, 2000; Hussmann et al., 2002; Segatz et al., 1988; Roberts and Nimmo, 2008), although it was also successfully applied to terrestrial planets (*e.g.,* Khan et al., 2018; Padovan et al., 2014). The drawback of the incompressibility assumption is that it can lead to large errors in the calculation of Love numbers for some applications, such as for large bodies where bulk deformations are relevant (Renaud and Henning, 2018) or bodies with a substantial melt fraction (Kervazo et al., 2021, 2022). The propagator method can be extended in a natural way to a spherically symmetric body modeled with uniform compressible layers (Sabadini et al., 2016). However, for a compressible layer, a closed-form expression for the fundamental matrix can be obtained only with the approximation that the gravity acceleration $g(r)$ scales linearly with r in each layer (*i.e.,* that the $g(r)/r$ ratio is constant), while an analytical form of the inverse of the fundamental matrix is not available (Vermeersen et al., 1996). Moreover, as discussed, for instance, by Hanyk et al. (1999) and Vermeersen and Mitrovica (2000), compressible viscoelastic models require particular attention due to the onset of gravitationally unstable modes known as Rayleigh–Taylor instabilities.

PyALMA^3 is based on the propagator approach. The methods used by PyALMA^3 to compute the Love numbers are presented in Melini et al. (2022). We briefly recall some of the most important details and equations, focusing on the evaluation of the frequency-dependent Love numbers relevant to planetary applications. Love numbers are obtained by solving the Laplace-transformed equilibrium equations at a given spherical harmonic degree n:

$$\mathbf{x}(s) = f(s)(P_1 \Lambda(s) J)(P_2 \Lambda(s) J)^{-1}\mathbf{b} \tag{12}$$

where $\mathbf{x}(s) = (u(s), v(s), \varphi(s))$ is the Laplace-transformed solution vector evaluated at the surface that contains the radial $u(s)$ and horizontal $v(s)$ displacements, and the variations of gravitational potential $\varphi(s)$, $f(s)$ describes the time-history of the forcing in the Laplace domain, P_1 and P_2 are projection operators, $\Lambda(s)$ contains the operators that propagate the solution from the core–mantle boundary to the outer surface, and J and $\mathbf{b}$ express the boundary conditions at the core–mantle boundary and the surface, respectively. The specific form of J depends on the assumed state of the core, *i.e.,* fluid inviscid or solid. The expressions of the propagators $\Lambda(s)$ and the operators P_1 and P_2 are given by Sabadini et al. (1982). Once an interior structure model is defined, the quantities in (12) can be computed, and the Love numbers derived from the solution vector $\mathbf{x}(s)$:

$$h_n(s) = \frac{M}{R} u(s) \tag{13}$$

$$l_n(s) = \frac{M}{R} v(s) \tag{14}$$

$$k_n(s) = -1 - \frac{M}{g_0 R} \varphi(s), \tag{15}$$

where M is the total mass of the body, R the surface radius, and $g_0 = g(R)$ the mean surface gravitational acceleration.

Global deformations of planetary bodies are usually induced by periodic external forcing such as tidal and loading potentials. In this context, equilibrium conditions (12) are computed at $s = j\omega$, where j is the imaginary unit, ω is the angular frequency of the forcing, and the Love numbers are derived by evaluating (13)-(15) at $s = j\omega$. As a result, Love numbers are complex, with the real part describing the strength of a planetary body and the imaginary part measuring the phase lag between the forcing and the response. Both parts can be measured by monitoring the effect of tidal deformation on the gravity field of the body.

Appendix B. Effects of bulk deformations

The main assumption underlying the matrix propagator method used by PyALMA^3 is that the layers are incompressible, *i.e.,* bulk deformations are neglected, which is equivalent to assuming an infinite bulk deformation modulus κ. Here, we test this assumption by comparing the tidal Love number k_2 computed for Europa with PyALMA^3 and the code used by Wahr et al. (2006), available as part of the SatStress code by Wahr et al. (2009) and modified from a previous code used to compute Earth's tides by Dahlen (1976). We adopt the four-layer modeling detailed in Section 2.2. For simplicity, we assume that the entire ice shell and the rock–metal core deform elastically.

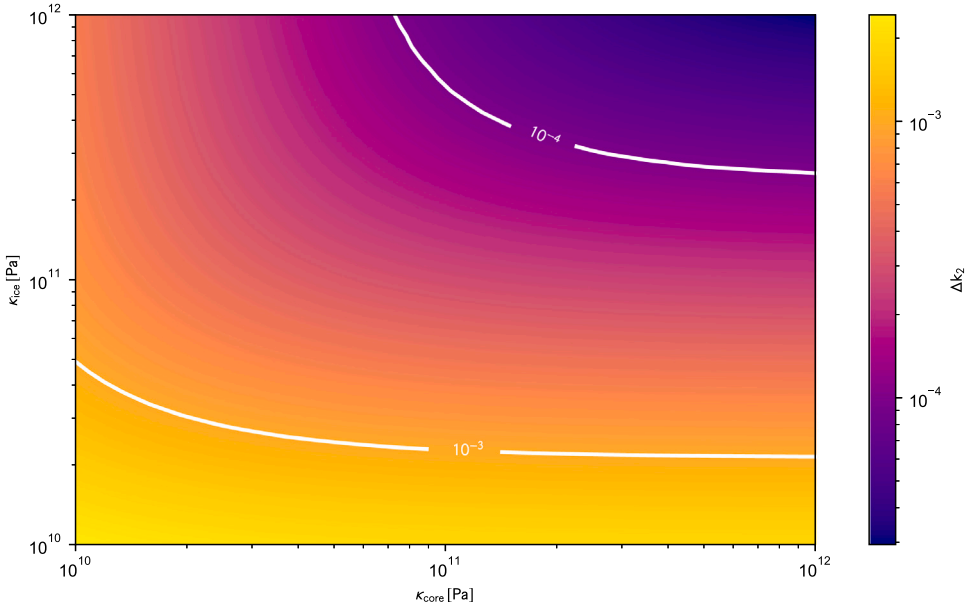

Fig. 8. Difference Δk_2 between the Love numbers computed with PyALMA^3 and with the tidal code by Wahr et al. (2006) as a function of ice shell and core bulk moduli. Δk_2 measures the effects of bulk deformations on the tidal response of Europa and is generally smaller than 10^{-3}, with a maximum difference between compressible and incompressible k_2 of 2.4×10^{-3} (corresponding to a relative difference of about 1%).

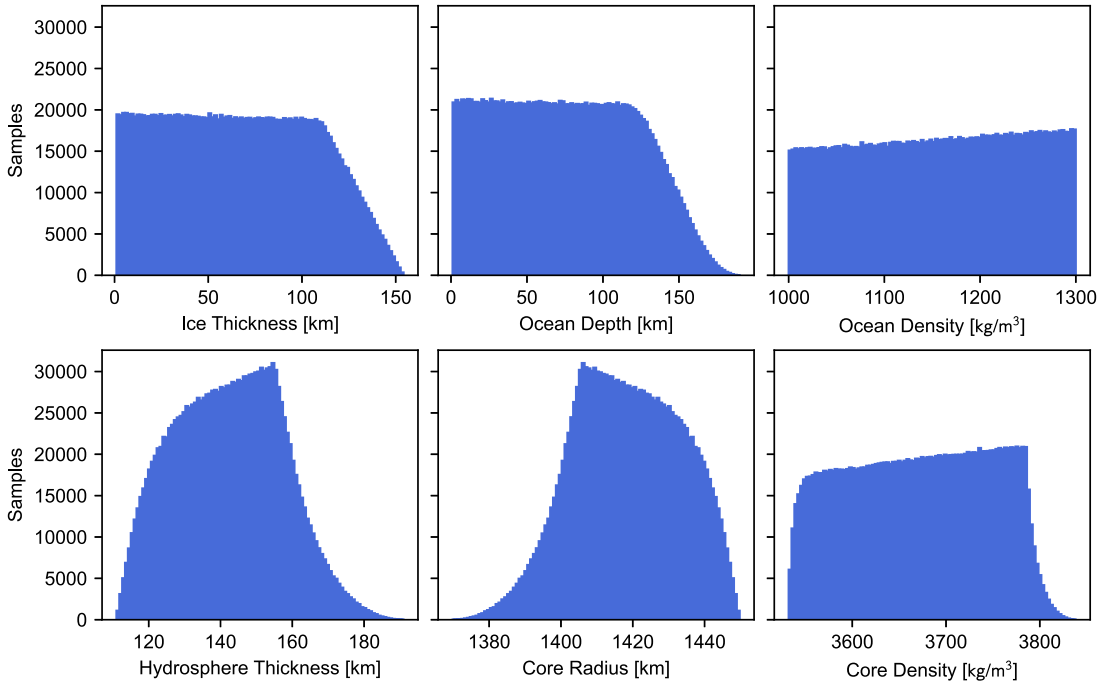

Fig. 9. Properties of the ice shell, ocean and rock-iron core of Europa after enforcing the constraints on the mass, radius, and MoI to the initial uniform distributions. All the models built from these distributions are consistent with observations and used to evaluate the tidal response of Europa.

The thicknesses of the ice and ocean are set to 30 km and 100 km, respectively, and their densities are 920 kg m^{-3} and 1000 kg m^{-3}. We vary the bulk moduli of all the ice and the core in order to understand their effects. The tidal code provided by Wahr et al. (2009) does not allow us to model the bulk deformations in the ocean, which is treated as a fluid layer in hydrostatic equilibrium. Furthermore, the response of the ocean is assumed to be static and any dynamic contribution is neglected (*e.g.*, Hay et al., 2022). Therefore, the tests carried out here are not conclusive regarding the tidal response of the ocean. The bulk moduli of the ice shell and the rock–metal core are varied at intervals $10^{10} - 10^{11}$ Pa and $10^{10} - 10^{12}$ Pa. The differences between PyALMA^3 and the code of Wahr et al. (2006) are reported in Fig. 8. We find that for Europa, the corrections to k_2 associated with compressible deformations are smaller than about 10^{-3} for most of the values of bulk moduli explored, with the maximum difference 2.4×10^{-3} (corresponding to a relative difference of about 1%). We also calculated the effects of bulk deformations on the tidal Love number h_2, reported in Figure S5. In this case, the relative differences are greater than for k_2, with a maximum correction of 7.5×10^{-3} that corresponds to a relative difference of about 7%. The effects on l_2 are similar and are not shown.

Appendix C. Resulting interior models of Europa

Our interior structure modeling uses broad boundaries as *a priori* information to build the uniform probability distributions that describe the interior properties. The constraints given by the observed mass, radius (enforced with the central values only without accounting for their uncertainties), and MoI (enforced with the $3-\sigma$ uncertainty) alter these uniform distributions. The resulting probability distributions are reported in Figure 9. These histograms show that using these constraints significantly narrows down the set of interior properties that can be used to evaluate the tidal response. For example, a sample extracted from the uniform distribution that describes the radius of the core before imposing the MoI constraint could range between $0-1560.8\,\mathrm{km}$ (*i.e.,*when both the ice shell and ocean thickness are randomly selected equal to 0). However, clearly these end-member models would not agree with the observations. Therefore, the radius of the interface between the deep interior and the ocean can only range between $1370-1450\,\mathrm{km}$ (Figure 9). Similarly, the thickness of the hydrosphere cannot be less than $111\,\mathrm{km}$ or larger than $191\,\mathrm{km}$ (Figure 9). We do not impose any boundary on the core density, which falls in the range $3532-3838\,\mathrm{kg\,m^{-3}}$ for all models, in agreement with the observations. All these results are consistent with previous investigations of Europa's interior based on 2, 3, or 4 layers (Anderson et al., 1998; Sohl et al., 2002; Petricca et al., 2023; Gomez Casajus et al., 2021). The properties of the ice layer and the ocean are not significantly altered with respect to the initial uniform distribution due to the well-known ambiguity in their determination from static gravity data (Petricca et al., 2023).

Appendix D. Supplementary data

Supplementary material related to this article can be found online at https://doi.org/10.1016/j.icarus.2024.116120.

References

Alterman, Z., Jarosch, H., Pekeris, C.L., 1959. Oscillations of the Earth. Proc. R. Soc. Lond. Ser. A Math. Phy. Sci. 252 (1268), 80–95. http://dx.doi.org/10.1098/rspa.1959.0138.

Amorim, D.O., Gudkova, T., 2024. Constraining Earth's mantle rheology with Love and Shida numbers at the M 2 tidal frequency. Phys. Earth Planet. Inter. 347, 107144. http://dx.doi.org/10.1016/j.pepi.2024.107144.

Anderson, J.D., Schubert, G., Jacobson, R.A., Lau, E.L., Moore, W.B., Sjogren, W.L., 1998. Europa's differentiated internal structure: Inferences from four Galileo encounters. Science 281 (5385), http://dx.doi.org/10.1126/science.281.5385.2019.

Andrade, E.N., 1910. On the viscous flow in metals, and allied phenomena. Proc. R. Soc. Lond. Ser. A, Containing Papers of a Mathematical and Physical Character 84 (567), 1–12. http://dx.doi.org/10.1098/rspa.1910.0050.

Ashkenazy, Y., 2019. The surface temperature of Europa. Heliyon 5, e01908. http://dx.doi.org/10.1016/j.heliyon.2019.e01908.

Bagheri, A., Efroimsky, M., Castillo-Rogez, J., Goossens, S., Plesa, A.C., Rambaux, N., Rhoden, A., Walterová, M., Khan, A., Giardini, D., 2022a. Tidal insights into rocky and icy bodies: an introduction and overview. In: Advances in Geophysics. pp. 231–320. http://dx.doi.org/10.1016/bs.agph.2022.07.004.

Bagheri, A., Khan, A., Al-Attar, D., Crawford, O., Giardini, D., 2019. Tidal response of Mars constrained from laboratory-based viscoelastic dissipation models and geophysical data. J. Geophys. Res.: Planets 124 (11), 2703–2727. http://dx.doi.org/10.1029/2019JE006015.

Bagheri, A., Khan, A., Deschamps, F., Samuel, H., Kruglyakov, M., Giardini, D., 2022b. The tidal–thermal evolution of the Pluto–Charon system. Icarus 376 (114871).

Běhounková, M., Tobie, G., Choblet, G., Kervazo, M., Melwani Daswani, M., Dumoulin, C., Vance, S.D., 2021. Tidally induced magmatic pulses on the oceanic floor of Jupiter's Moon Europa. Geophys. Res. Lett. 48 (3), http://dx.doi.org/10.1029/2020GL090077.

Bierson, C.J., 2024. The impact of rheology model choices on tidal heating studies. Icarus 414, 116026. http://dx.doi.org/10.1016/j.icarus.2024.116026.

Bills, B.G., 2005. Improved estimate of tidal dissipation within Mars from MOLA observations of the shadow of Phobos. J. Geophys. Res. 110 (E7), E07004. http://dx.doi.org/10.1029/2004JE002376.

Biot, M.A., 1954. Theory of stress–strain relations in anisotropic viscoelasticity and relaxation phenomena. J. Appl. Phys. 25 (11), 1385–1391. http://dx.doi.org/10.1063/1.1721573.

Bray, V.J., Collins, G.S., Morgan, J.V., Melosh, H.J., Schenk, P.M., 2014. Hydrocode simulation of Ganymede and Europa cratering trends – How thick is Europa's crust? Icarus 231, 394–406. http://dx.doi.org/10.1016/j.icarus.2013.12.009.

Briaud, A., Fienga, A., Melini, D., Rambaux, N., Mémin, A., Spada, G., Saliby, C., Hussmann, H., Stark, A., Viswanathan, V., Baguet, D., 2023a. Constraints on the lunar core viscosity from tidal deformation. Icarus 394, 115426. http://dx.doi.org/10.1016/j.icarus.2023.115426.

Briaud, A., Ganino, C., Fienga, A., Mémin, A., Rambaux, N., 2023b. The lunar solid inner core and the mantle overturn. Nature 617 (7962), 743–746. http://dx.doi.org/10.1038/s41586-023-05935-7.

Cappuccio, P., Di Benedetto, M., Durante, D., Iess, L., 2022. Callisto and Europa gravity measurements from JUICE 3GM experiment simulation. Planet. Sci. J. 3 (8), 199. http://dx.doi.org/10.3847/PSJ/ac83c4.

Cappuccio, P., Hickey, A., Durante, D., Di Benedetto, M., Iess, L., De Marchi, F., Plainaki, C., Milillo, A., Mura, A., 2020. Ganymede's gravity, tides and rotational state from JUICE's 3GM experiment simulation. Planet. Space Sci. 187, 104902. http://dx.doi.org/10.1016/j.pss.2020.104902.

Castillo-Rogez, J.C., Efroimsky, M., Lainey, V., 2011. The tidal history of Iapetus: Spin dynamics in the light of a refined dissipation model. J. Geophys. Res.: Planets 116 (E9), http://dx.doi.org/10.1029/2010JE003664.

Choukroun, M., Grasset, O., 2007. Thermodynamic model for water and high-pressure ices up to 2.2GPa and down to the metastable domain. J. Chem. Phys. 127 (12), http://dx.doi.org/10.1063/1.2768957.

Cole, D.M., Durell, G.D., 1995. The cyclic loading of saline ice. Phil. Mag. A 72, 209–229. http://dx.doi.org/10.1080/01418619508239591.

Dahlen, F.A., 1976. The passive influence of the oceans upon the rotation of the Earth. Geophys. J. Int. 46 (2), 363–406. http://dx.doi.org/10.1111/j.1365-246X.1976.tb04163.x.

Deschamps, F., Sotin, C., 2001. Thermal convection in the outer shell of large icy satellites. J. Geophys. Res.: Planets 106 (E3), 5107–5121. http://dx.doi.org/10.1029/2000JE001253.

Dmitrovskii, A.A., Khan, A., Boehm, C., Bagheri, A., van Driel, M., 2022. Constraints on the interior structure of Phobos from tidal deformation modeling. Icarus 372, 114714.

Dumoulin, C., Tobie, G., Verhoeven, O., Rosenblatt, P., Rambaux, N., 2017. Tidal constraints on the interior of Venus. J. Geophys. Res.: Planets 122 (6), 1338–1352. http://dx.doi.org/10.1002/2016JE005249.

Efroimsky, M., 2012. Tidal dissipation compared to seismic dissipation: in small bodies, Earths, and Super-Earths. Astrophys. J. 746 (2), 150. http://dx.doi.org/10.1088/0004-637X/746/2/150.

Farrell, W.E., 1972. Deformation of the Earth by surface loads. Rev. Geophys. 10 (3), 761. http://dx.doi.org/10.1029/RG010i003p00761.

Fukusako, S., 1990. Thermophysical properties of ice, snow, and sea ice. Int. J. Thermophys. 11 (2), 353–372. http://dx.doi.org/10.1007/BF01133567.

Genova, A., Goossens, S., Mazarico, E., Lemoine, F.G., Neumann, G.A., Kuang, W., Sabaka, T.J., Hauck, S.A., Smith, D.E., Solomon, S.C., Zuber, M.T., 2019. Geodetic evidence that mercury has a solid inner core. Geophys. Res. Lett. 46, 3625–3633. http://dx.doi.org/10.1029/2018GL081135.

Genova, A., Parisi, M., Gargiulo, A.M., Petricca, F., Andolfo, S., Torrini, T., Vecchio, E.D., Glein, C.R., Cable, M.L., Phillips, C.B., Bradley, N.E., Restrepo, R.L., Mages, D.M., Babuscia, A., Lunine, J.I., 2024. Gravity investigation to characterize enceladus's ocean and interior. Planet. Sci. J. 5, 40. http://dx.doi.org/10.3847/PSJ/ad16df.

Gevorgyan, Y., Boué, G., Ragazzo, C., Ruiz, L.S., Correia, A.C., 2020. Andrade rheology in time-domain. Application to Enceladus' dissipation of energy due to forced libration. Icarus 343, 113610. http://dx.doi.org/10.1016/j.icarus.2019.113610.

Goldsby, D.L., Kohlstedt, D.L., 2001. Superplastic deformation of ice: Experimental observations. J. Geophys. Res.: Solid Earth 106 (B6), 11017–11030. http://dx.doi.org/10.1029/2000JB900336.

Gomez Casajus, L., Zannoni, M., Modenini, D., Tortora, P., Nimmo, F., Van Hoolst, T., Buccino, D., Oudrhiri, K., 2021. Updated Europa gravity field and interior structure from a reanalysis of Galileo tracking data. Icarus 358, http://dx.doi.org/10.1016/j.icarus.2020.114187.

Goossens, S., Renaud, J.P., Henning, W.G., Mazarico, E., Bertone, S., Genova, A., 2022. Evaluation of recent measurements of Mercury's moments of inertia and tides using a comprehensive Markov chain Monte Carlo method. Planet. Sci. J. 3 (2), 37. http://dx.doi.org/10.3847/PSJ/ac4bb8.

Hand, K.P., Chyba, C.F., 2007. Empirical constraints on the salinity of the Europan ocean and implications for a thin ice shell. Icarus 189 (2), 424–438. http://dx.doi.org/10.1016/j.icarus.2007.02.002.

Hanyk, L., Matyska, C., Yuen, D.A., 1999. Secular gravitational instability of a compressible viscoelastic sphere. Geophys. Res. Lett. 26 (5), 557–560. http://dx.doi.org/10.1029/1999GL900024.

Hay, H.C.F.C., Matsuyama, I., Pappalardo, R.T., 2022. The high-frequency tidal response of ocean worlds: Application to Europa and Ganymede. J. Geophys. Res.: Planets 127, http://dx.doi.org/10.1029/2021JE007064.

Howell, S.M., 2021. The likely thickness of Europa's icy shell. Planet. Sci. J. 2 (4), 129. http://dx.doi.org/10.3847/PSJ/abfe10.

Hussmann, H., Spohn, T., Wieczerkowski, K., 2002. Thermal equilibrium states of Europa's ice shell: Implications for internal ocean thickness and surface heat flow. Icarus 156 (1), 143–151. http://dx.doi.org/10.1006/icar.2001.6776.

Iess, L., Jacobson, R.A., Ducci, M., Stevenson, D.J., Lunine, J.I., Armstrong, J.W., Asmar, S.W., Racioppa, P., Rappaport, N.J., Tortora, P., 2012. The tides of Titan. Science 337 (6093), 457–459. http://dx.doi.org/10.1126/science.1219631.

Jackson, I., Faul, U.H., Skelton, R., 2014. Elastically accommodated grain-boundary sliding: New insights from experiment and modeling. Phys. Earth Planet. Inter. 228, 203–210.

Journaux, B., Brown, J.M., Pakhomova, A., Collings, I.E., Petitgirard, S., Espinoza, P., Boffa Ballaran, T., Vance, S.D., Ott, J., Cova, F., Garbarino, G., Hanfland, M., 2020. Holistic approach for studying planetary hydrospheres: Gibbs representation of ices thermodynamics, elasticity, and the water phase diagram to 2,300 MPa. J. Geophys. Res.: Planets 125 (1), http://dx.doi.org/10.1029/2019JE006176.

Kamata, S., Kimura, J., Matsumoto, K., Nimmo, F., Kuramoto, K., Namiki, N., 2016. Tidal deformation of Ganymede: Sensitivity of Love numbers on the interior structure. J. Geophys. Res.: Planets 121, 1362–1375. http://dx.doi.org/10.1002/2016JE005071.

Kargel, J.S., Kaye, J.Z., Head, J.W., Marion, G.M., Sassen, R., Crowley, J.K., Ballesteros, O.P., Grant, S.A., Hogenboom, D.L., 2000. Europa's crust and ocean: Origin, composition, and the prospects for life. Icarus 148 (1), 226–265. http://dx.doi.org/10.1006/icar.2000.6471.

Kervazo, M., Tobie, G., Choblet, G., Dumoulin, C., Běhounková, M., 2021. Solid tides in Io's partially molten interior. Astron. Astrophys. 650, A72. http://dx.doi.org/10.1051/0004-6361/202039433.

Kervazo, M., Tobie, G., Choblet, G., Dumoulin, C., Běhounková, M., 2022. Inferring Io's interior from tidal monitoring. Icarus 373, 114737. http://dx.doi.org/10.1016/j.icarus.2021.114737.

Khan, A., Liebske, C., Rozel, A., Rivoldini, A., Nimmo, F., Connolly, J.A.D., Plesa, A.C., Giardini, D., 2018. A geophysical perspective on the bulk composition of Mars. J. Geophys. Res.: Planets 123 (2), 575–611. http://dx.doi.org/10.1002/2017JE005371.

Love, A.E.H., 1911. Some problems of geodynamics. Dover, New York.

Mazarico, E., Buccino, D., Castillo-Rogez, J., Dombard, A.J., Genova, A., Hussmann, H., Kiefer, W.S., Lunine, J.I., McKinnon, W.B., Nimmo, F., Park, R.S., Roberts, J.H., Srinivasan, D.K., Steinbrügge, G., Tortora, P., Withers, P., 2023. The Europa clipper gravity and radio science investigation. Space Sci. Rev. 219 (4), 30. http://dx.doi.org/10.1007/s11214-023-00972-0.

McDougall, T.J., Barker, P.M., 2011. Getting started with TEOS-10 and the Gibbs Seawater (GSW) oceanographic toolbox. SCOR/IAPSO WG.

McKinnon, W.B., 1999. Convective instability in Europa's floating ice shell. Geophys. Res. Lett. 26 (7), 951–954. http://dx.doi.org/10.1029/1999GL900125.

Melini, D., Saliby, C., Spada, G., 2022. On computing viscoelastic Love numbers for general planetary models: the <tt>ALMA3</tt> code. Geophys. J. Int. 231 (3), 1502–1517. http://dx.doi.org/10.1093/gji/ggac263.

Michel, A., Boy, J.-P., 2021. Viscoelastic Love numbers and long-period geophysical effects. Geophys. J. Int. 228 (2), 1191–1212. http://dx.doi.org/10.1093/gji/ggab369.

Mitri, G., Meriggiola, R., Hayes, A., Lefevre, A., Tobie, G., Genova, A., Lunine, J.I., Zebker, H., 2014. Shape, topography, gravity anomalies and tidal deformation of Titan. Icarus 236, 169–177. http://dx.doi.org/10.1016/j.icarus.2014.03.018.

Moore, W.B., 2006. Thermal equilibrium in Europa's ice shell. Icarus 180 (1), 141–146. http://dx.doi.org/10.1016/j.icarus.2005.09.005.

Moore, W.B., Schubert, G., 2000. The tidal response of Europa. Icarus 147 (1), 317–319. http://dx.doi.org/10.1006/icar.2000.6460.

Nimmo, F., Faul, U.H., 2013. Dissipation at tidal and seismic frequencies in a melt-free, anhydrous Mars. J. Geophys. Res.: Planets 118 (12), 2558–2569.

Ojakangas, G.W., Stevenson, D.J., 1989. Thermal state of an ice shell on Europa. Icarus 81, 220–241.

Padovan, S., Margot, J.-L., Hauck, S.A., Moore, W.B., Solomon, S.C., 2014. The tides of Mercury and possible implications for its interior structure. J. Geophys. Res.: Planets 119 (4), 850–866. http://dx.doi.org/10.1002/2013JE004459.

Pappalardo, R.T., Head, J.W., Greeley, R., Sullivan, R.J., Pilcher, C., Schubert, G., Moore, W.B., Carr, M.H., Moore, J.M., Belton, M.J.S., Goldsby, D.L., 1998. Geological evidence for solid-state convection in Europa's ice shell. Nature 391 (6665), 365–368. http://dx.doi.org/10.1038/34862.

Peltier, W.R., 1974. The impulse response of a Maxwell Earth. Rev. Geophys. 12 (4), 649. http://dx.doi.org/10.1029/RG012i004p00649.

Petricca, F., Genova, A., Castillo-Rogez, J.C., Styczinski, M.J., Cochrane, C.J., Vance, S.D., 2023. Characterization of icy moon hydrospheres through joint inversion of gravity and magnetic field measurements. Geophys. Res. Lett. 50 (17), http://dx.doi.org/10.1029/2023GL104016.

Petricca, F., Genova, A., Goossens, S., Iess, L., Spada, G., 2022. Constraining the internal structures of Venus and Mars from the gravity response to atmospheric loading. Planet. Sci. J. 3 (7), 164. http://dx.doi.org/10.3847/PSJ/ac7878.

Rambaux, N., Castillo-Rogez, J.C., Williams, J.G., Karatekin, Ö., 2010. Librational response of Enceladus. Geophys. Res. Lett. 37 (4), http://dx.doi.org/10.1029/2009GL041465.

Renaud, J.P., Henning, W.G., 2018. Increased tidal dissipation using advanced rheological models: Implications for Io and tidally active exoplanets. Astrophys. J. 857 (2), 98. http://dx.doi.org/10.3847/1538-4357/aab784.

Renaud, J.P., Henning, W.G., Saxena, P., Neveu, M., Bagheri, A., Mandell, A., Hurford, T., 2021. Tidal dissipation in dual-body, highly eccentric, and non-synchronously rotating systems: Applications to Pluto–Charon and the exoplanet TRAPPIST-1e. Planet. Sci. J. 2 (1), 4.

Roberts, J.H., McKinnon, W.B., Elder, C.M., Tobie, G., Biersteker, J.B., Young, D., Park, R.S., Steinbrügge, G., Nimmo, F., Howell, S.M., Castillo-Rogez, J.C., Cable, M.L., Abrahams, J.N., Bland, M.T., Chivers, C., Cochrane, C.J., Dombard, A.J., Ernst, C., Genova, A., Gerekos, C., Glein, C., Harris, C.D., Hay, H.C.F.C., Hayne, P.O., Hedman, M., Hussmann, H., Jia, X., Khurana, K., Kiefer, W.S., Kirk, R., Kivelson, M., Lawrence, J., Leonard, E.J., Lunine, J.I., Mazarico, E., McCord, T.B., McEwen, A., Paty, C., Quick, L.C., Raymond, C.A., Retherford, K.D., Roth, L., Rymer, A., Saur, J., Scanlan, K., Schroeder, D.M., Senske, D.A., Shao, W., Soderlund, K., Spiers, E., Styczinski, M.J., Tortora, P., Vance, S.D., Villarreal, M.N., Weiss, B.P., Westlake, J.H., Withers, P., Wolfenbarger, N., Buratti, B., Korth, H., Pappalardo, R.T., 2023. Exploring the interior of Europa with the Europa clipper. Space Sci. Rev. 219 (6), 46. http://dx.doi.org/10.1007/s11214-023-00990-y.

Roberts, J.H., Nimmo, F., 2008. Tidal heating and the long-term stability of a subsurface ocean on Enceladus. Icarus 194 (2), 675–689. http://dx.doi.org/10.1016/j.icarus.2007.11.010.

Ruiz, J., 2005. The heat flow of Europa. Icarus 177 (2), 438–446. http://dx.doi.org/10.1016/j.icarus.2005.03.021.

Sabadini, R., Vermeersen, B., Cambiotti, G., 2016. Global Dynamics of the Earth: Applications of Viscoelastic Relaxation Theory to Solid-Earth and Planetary Geophysics. Springer Netherlands, Dordrecht, http://dx.doi.org/10.1007/978-94-017-7552-6.

Sabadini, R., Yuen, D.A., Boschi, E., 1982. Polar wandering and the forced responses of a rotating, multilayered, viscoelastic planet. J. Geophys. Res. 87 (B4), 2885. http://dx.doi.org/10.1029/JB087iB04p02885.

Saliby, C., Fienga, A., Briaud, A., Mémin, A., Herrera, C., 2023. Viscosity contrasts in the Venus mantle from tidal deformations. Planet. Space Sci. 231, 105677. http://dx.doi.org/10.1016/j.pss.2023.105677.

Segatz, M., Spohn, T., Ross, M., Schubert, G., 1988. Tidal dissipation, surface heat flow, and figure of viscoelastic models of Io. Icarus 75 (2), 187–206. http://dx.doi.org/10.1016/0019-1035(88)90001-2.

Sohl, F., Spohn, T., Breuer, D., Nagel, K., 2002. Implications from Galileo observations on the interior structure and chemistry of the Galilean satellites. Icarus 157, 104–119. http://dx.doi.org/10.1006/icar.2002.6828.

Solomatov, V.S., 1995. Scaling of temperature- and stress-dependent viscosity convection. Phys. Fluids 7 (2), 266–274. http://dx.doi.org/10.1063/1.868624.

Spada, G., 2008. ALMA, a Fortran program for computing the viscoelastic Love numbers of a spherically symmetric planet. Comput. Geosci. 34 (6), 667–687. http://dx.doi.org/10.1016/j.cageo.2007.12.001.

Spearman, C., 1904. The proof and measurement of association between two things. Am. J. Psychol. 15 (1), 72. http://dx.doi.org/10.2307/1412159.

Spencer, J.R., Tamppari, L.K., Martin, T.Z., Travis, L.D., 1999. Temperatures on Europa from galileo photopolarimeter-radiometer: Nighttime thermal anomalies. Science 284, 1514–1516. http://dx.doi.org/10.1126/science.284.5419.1514.

Steinbrügge, G., Schroeder, D., Haynes, M., Hussmann, H., Grima, C., Blankenship, D., 2018. Assessing the potential for measuring Europa's tidal Love number h2 using radar sounder and topographic imager data. Earth Planet. Sci. Lett. 482, 334–341. http://dx.doi.org/10.1016/j.epsl.2017.11.028.

Styczinski, M.J., Melini, D., Tharimena, S., 2024. drsaikirant88/PyALMA3: Public release along with manuscript submission. http://dx.doi.org/10.5281/zenodo.10472443, URL: https://github.com/drsaikirant88/PyALMA3.

Styczinski, M.J., Vance, S.D., Melwani Daswani, M., 2023a. PlanetProfile: Self-consistent interior structure modeling for ocean worlds and rocky dwarf planets in python. Earth Space Sci. 10 (8), http://dx.doi.org/10.1029/2022EA002748.

Styczinski, M.J., Vance, S.D., Niesyt, M., Lisitsyn, A., Daswani, M.M., Marusiak, A.G., Vega, K., Bryant, A.S., 2023b. vancesteven/PlanetProfile. http://dx.doi.org/10.5281/zenodo.844130.

Sundberg, M., Cooper, R.F., 2010. A composite viscoelastic model for incorporating grain boundary sliding and transient diffusion creep; correlating creep and attenuation responses for materials with a fine grain size. Phil. Mag. 90 (20), 2817–2840. http://dx.doi.org/10.1080/14786431003746656.

Takeuchi, H., Saito, M., 1972. Seismic Surface Waves. In: Bolt, B.A. (Ed.), Seismology: Surface Waves and Earth Oscillations. pp. 217–295. http://dx.doi.org/10.1016/B978-0-12-460811-5.50010-6.

Tobie, G., Mocquet, A., Sotin, C., 2005. Tidal dissipation within large icy satellites: Applications to Europa and Titan. Icarus 177 (2), 534–549. http://dx.doi.org/10.1016/j.icarus.2005.04.006.

Vance, S., Bouffard, M., Choukroun, M., Sotin, C., 2014. Ganymede's internal structure including thermodynamics of magnesium sulfate oceans in contact with ice. Planet. Space Sci. 96, 62–70. http://dx.doi.org/10.1016/j.pss.2014.03.011.

Vance, S., Brown, J.M., 2013. Thermodynamic properties of aqueous $MgSO_4$ to 800 MPa at temperatures from -20 to 100 °C and concentrations to 2.5 mol kg^{-1} from sound speeds, with applications to icy ocean world oceans. Geochim. Cosmochim. Acta 110, 176–189. http://dx.doi.org/10.1016/j.gca.2013.01.040.

Vance, S.D., Panning, M.P., Stähler, S., Cammarano, F., Bills, B.G., Tobie, G., Kamata, S., Kedar, S., Sotin, C., Pike, W.T., Lorenz, R., Huang, H.H., Jackson, J.M., Banerdt, B., 2018. Geophysical Investigations of Habitability in Ice-Covered Ocean Worlds. J. Geophys. Res.: Planets 123 (1), 180–205. http://dx.doi.org/10.1002/2017JE005341.

Vance, S.D., Styczinski, M.J., Bills, B.G., Cochrane, C.J., Soderlund, K.M., Gómez-Pérez, N., Paty, C., 2021. Magnetic induction responses of Jupiter's ocean moons including effects from adiabatic convection. J. Geophys. Res.: Planets 126 (2), http://dx.doi.org/10.1029/2020JE006418, e2020JE006418.

Vermeersen, L., Mitrovica, J., 2000. Gravitational stability of spherical self-gravitating relaxation models. Geophys. J. Int. 142 (2), 351–360. http://dx.doi.org/10.1046/j.1365-246x.2000.00159.x.

Vermeersen, L.L.A., Sabadini, R., Spada, G., 1996. Compressible rotational deformation. Geophys. J. Int. 126, 735–761.

Vilella, K., Choblet, G., Tsao, W.-E., Deschamps, F., 2020. Tidally heated convection and the occurrence of melting in icy satellites: Application to Europa. J. Geophys. Res.: Planets 125 (3), http://dx.doi.org/10.1029/2019JE006248.

Wahr, J., Selvans, Z.A., Mullen, M.E., Barr, A.C., Collins, G.C., Selvans, M.M., Pappalardo, R.T., 2009. Modeling stresses on satellites due to nonsynchronous rotation and orbital eccentricity using gravitational potential theory. Icarus 200 (1), 188–206. http://dx.doi.org/10.1016/j.icarus.2008.11.002.

Wahr, J., Zuber, M.T., Smith, D.E., Lunine, J.I., 2006. Tides on Europa, and the thickness of Europa's icy shell. J. Geophys. Res.: Planets 111 (E12), http://dx.doi.org/10.1029/2006JE002729.

Walterová, M., Plesa, A.-C., Wagner, F.W., Breuer, D., 2023. Andrade rheology in planetary science. Authorea Preprints.

Yoder, C.F., Konopliv, A.S., Yuan, D.N., Standish, E.M., Folkner, W.M., 2003. Fluid core size of Mars from detection of the solar tide. Science 300 (5617), 299–303. http://dx.doi.org/10.1126/science.1079645.

Zimmer, C., Khurana, K.K., Kivelson, M.G., 2000. Subsurface oceans on Europa and Callisto: Constraints from Galileo magnetometer observations. Icarus 147 (2), 329–347. http://dx.doi.org/10.1006/icar.2000.6456.